

# Safeguarding Venice from high tides: site characterization & geotechnical problems

## La sauvegarde de Venise des hautes-marées: caractérisation du site et problèmes géotechniques

M. Jamiolkowski

Technical University of Torino, M.Jamiolkowski@polito.it

G. Ricceri

Department IMAGE, University of Padova, giuseppe.ricceri@unipd.it

P. Simonini

Department IMAGE, University of Padova, paolo.simonini@unipd.it

### ABSTRACT

The historical city of Venice is threatened by frequent flooding caused by the eustatic rise of the sea level and due to subsidence, so that this city, one of the most visited in the world, is put at risk by the very element that makes it famous: its canals which can no longer contain the rise of the tidal waters. This paper briefly describes the remedial actions undertaken to safeguard the city and its inhabitants against any damage to their regular activities and to the tourism. The geotechnical issues related to the safeguard measures being implemented are also discussed.

### RÉSUMÉ

La ville historique de Venise est menacée par des fréquents inondations provoquées par la montée eustatique du niveau de la mer et par la subsidence, qui mettent au risque la ville, une des plus visitées au monde, pour le même élément qui la fait célèbre: ses canaux qui ne peuvent plus contenir les eaux de haute-marée. Cet article donne une bref description des travaux de confortement mis en œuvre pour préserver la ville et ses habitants contre tous dommages aux activités habituelles et au tourisme. Les aspects géotechniques en relation avec les mesures de confortement en cours de réalisation sont aussi exposés.

Keywords: Venice, high tides, site characterization, safeguarding measures, foundation design.

## 1 GENERAL INFORMATION

The city of Venice and the surrounding Lagoon sites are subject to high tides floods which have grown steadily more frequent and higher since early 1900's.

The normal tide height in the Lagoon reaches elevations ranging from 0.4 m to 0.6 m above the Punta Della Salute datum, located opposite San Marco Square. Flooding occurs mainly during fall and winter, in concurrence with low atmospheric pressure, strong winds blowing from Adriatic Sea and enduring rain.

During the last century sea level has risen and land level has dropped; as a result, Venice has "lost" 240 mm with respect to the sea, and floods have become more recurrent and intense. This phenomenon (Fig. 1) has been triggered by the eustatic rise of the sea level, the natural subsidence, and since mid 1920s by the additional subsidence due to water extraction. In early 1970s the water extraction from the wells in the Venice and Mestre area was forbidden; after a moderate rebound, the subsidence went back to its natural trend.

Fig. 2 displays the tides exceeding +1.1 m occurrence in the period 1923-2003, and the elevations reached by some exceptionally high tides since 1951.

When tides exceed +1.00 m Piazza San Marco, the area adjacent Doge's Palace and the San Marco's banks are flooded. When tides exceed +1.20 and 1.40+m, respectively 40% and more than 60% of the city area is flooded.

The increased tidal flooding is becoming a real threat for Venice, its citizens and visitors; furthermore, the phenomenon will get worse with time. Accordingly, since 1970s studies and investigations have been carried out to defend Venice and the entire Lagoon site.

A long term safeguarding project was approved in early 1990, including the erosion mitigation, the morphological restoration of the coast line, the renovation of the existing jetties, the fishing farms re-opening and the oil tankers traffic reduction.

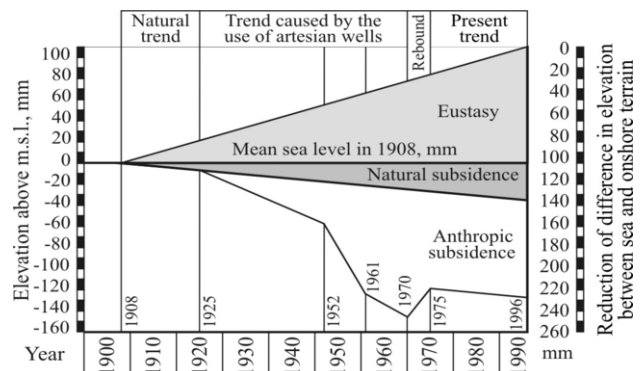


Figure 1. Eustatic rise of the sea level, the natural subsidence.

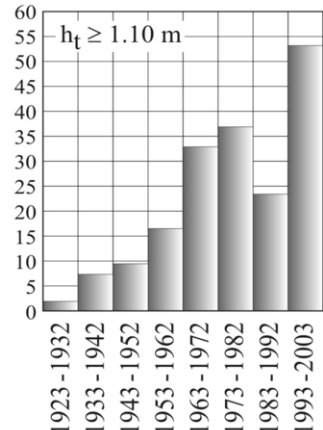
Highest tides recorded\*, m

|          |      |      |
|----------|------|------|
| December | 2008 | 1.56 |
| November | 2007 | 1.08 |
| November | 2006 | 1.14 |
| December | 2005 | 1.32 |
| November | 2004 | 1.38 |
| January  | 2003 | 1.34 |
| November | 2002 | 1.47 |
| November | 2000 | 1.44 |
| December | 1992 | 1.42 |
| February | 1986 | 1.59 |
| December | 1979 | 1.66 |
| February | 1979 | 1.40 |
| November | 1968 | 1.44 |
| November | 1966 | 1.94 |
| October  | 1960 | 1.45 |
| November | 1951 | 1.51 |

(\* ) As referred to Punta della Salute datum.

Figure 2. Trend of tides.

Number of high water events



In the following only the interventions aimed at safeguarding Venice from flooding will be presented and will be grouped as follow:

- Mobile barriers project (MOSE: acronym for Modulo Sperimentale Elettromeccanico: Experimental Electromechanical Module). it consists in a series of caissons embedded under the sea bottom at the three lagoon inlets, and housing flap gates ensuring the closure of the inlets when a high tide of elevation +1.10 m or higher is forecasted (Fig. 3). The project is promoted by the Italian Ministry of Infrastructures, locally represented by the Venice Water Authority. The work has been assigned to some of the main Italian contractors, associated in a Consortium, named: Consorzio Venezia Nuova, Technital Engineering Group, based in Verona and Milano, has been appointed as general designer.
- Insulae Project, consisting in raising the elevation of banks, pavements and sidewalks in some selected areas, to prevent the floods generated by tides within +1.00 m. A typical example is the protection of San Marco Square reported by Burghignoli et al. (2007)

2 SITE CHARACTERIZATION

In the last three decades, comprehensive geotechnical studies have been carried out to characterize the Lagoon soils at the inlets.

Geotechnical investigations were performed in the late 1980s to draw the relevant soil profiles along with the cross sections of the three lagoon inlets and to estimate the significant geotechnical properties for a preliminary selection of the barriers foundations. To accomplish a proper foundation design they were integrated, between 2001 and 2004, with additional and more exhaustive investigations, whose types and numbers are reported in Fig. 4.

Based on preliminary geological and geotechnical investigations, it was recognized that the key lagoon soils characteristic is the presence of a predominant silt fraction, combined with clay and/or sand forming a chaotic interbedding of different sediments. The basic mineralogical components of the lagoon sediments only just vary, as a result of similar geological origins and common depositional environment. This feature, together with the considerable heterogeneity of the soil layering, suggested also to focus the research mainly on some selected trial tests sites, considered as representative of the typical soil profiles, where relevant in-situ and laboratory investigations could be carried out for a more detailed characterization of the Lagoon soils.

The first test site, specifically the Malamocco Test Site (MTS) (Cola & Simonini 1999, 2002; Ricceri et al. 2002) was located at the Malamocco inlet. Within a limited area, a series of investigations that included boreholes, piezocone (CPTU), dilatometer (DMT), self-boring pressuremeter (SBPM) and cross hole tests (CHT) were performed on contiguous locations. One of the main aims of the MTS was to calibrate, for the lagoon deposits, the empirical correlations between the soil classification and its mechanical properties based on CPTU and DMT results, including their versions (SCPTU, SDMT) allowing to measure also the shear wave velocity  $V_s$ .

Due to the influence of the pronounced soil heterogeneity, substantial technical hitches were met in assessing the significant soil properties directly from in situ site tests. The comprehensive laboratory test program completed at MTS emphasized the very heterogeneous nature of the Lagoon soils. In addition, because of the high silt content the sediments resulted extremely sensitive to stress relief and disturbance due to sampling, thus affecting negatively evaluation and reliability of laboratory tests.

A new test site was therefore selected, namely the Treporti Test Site (TTS) (Simonini 2004, Simonini et al. 2006, Ricceri, 2007), located at the inner border of the lagoon, very close to

the Lido inlet. Its purpose was to assess directly in situ the stress-strain-time properties of the heterogeneous Lagoon soils. At the TTS a vertically-walled circular embankment, loading up the ground to 107 kPa, was constructed across 2002 and 2003, measuring, during and after the construction, the relevant ground displacements together with the pore pressure evolution. After 6 years at a constant load, the bank was completely removed.

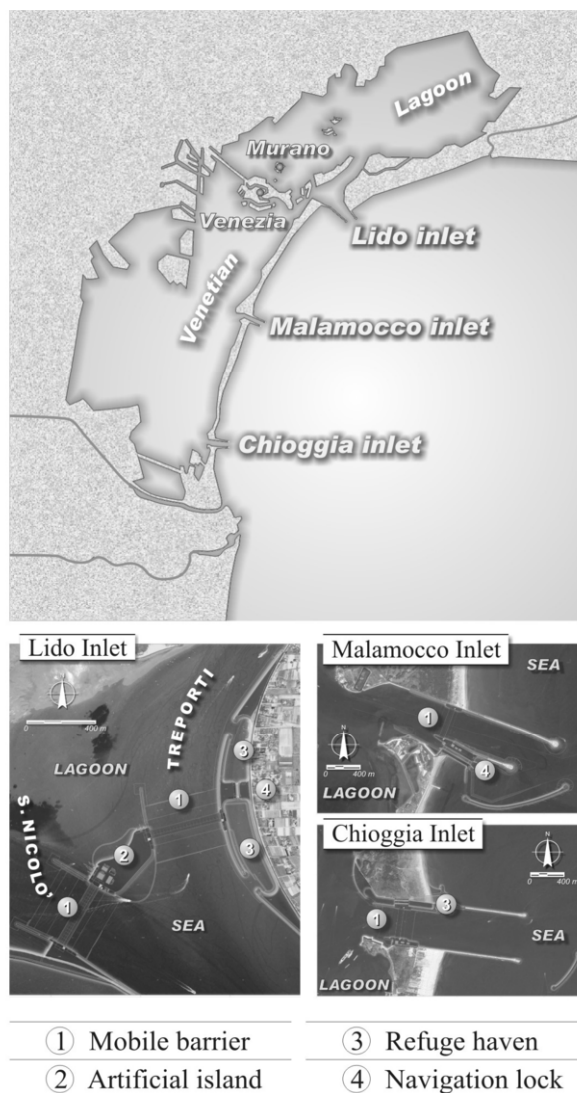


Figure 3. MOSE

|   |                        |
|---|------------------------|
| <b>BH</b>   | <b>DMT</b>             |
| n°88, depth 40 to 120 m   | n°11, depth 50 m       |
| <b>CPTU</b>   | <b>SPT-BH</b>          |
| n° 119, depth 30 to 120 m   | n°13, depth 40 to 50 m |
| <p><b>BH</b> Geotechnical borings; undisturbed sampling, <b>SPT</b>'s, <b>FVT</b>'s<br/> <b>CPTU</b> Static Cone Penetration Test with pore pressure measurement<br/> <b>DMT</b> Marchetti's Flat Dilatometer Test<br/> <b>SPT-BH</b> Standard Penetration Test, carried out in dedicated 3" O.D. holes</p> |                        |
| <ul style="list-style-type: none"> <li>• Undisturbed samples retrieved by means of Osterberg Piston Sampler 98 mm O.D.</li> <li>• 3 CH tests carried out, each employing three 80 deep-holes</li> <li>• Rod energy measured in one of SPT-BH, ER = 63%</li> </ul>   |                        |

Figure 4. Site investigation for the final design stage (2001 to 2004).

The ground beneath the embankment was heavily instrumented with rod extensometers, sliding deformeters, (Kovari and Amstad (1982), GPS, inclinometers, piezometers and load cells. Boreholes with undisturbed sampling, traditional CPTU (Gottardi & Tonni 2004) and DMT (Marchetti et al. 2004), seismic SCPTU and SDMT (Mayne & McGillivray 2004) were carried out to characterize the subsoil profile and estimate the soil mechanical properties.

During the Quaternary Era the lagoon underwent some discontinuous phases of alternating marine transgression and regression, as a result of which both marine and continental sediments coexist. As shown in Fig. 5, [Belloni and Caielli (1997)], in the upper 80 m below the sea bottom, the lagoon deposits, characterized by a complex system of interbedded sands, silts and silty clays with inclusions of peat, belong to the upper Pleistocene and are covered by the most recent Holocene sediments, whose thickness ranges between 8 and 15 m.

The contact between Pleistocene and Holocene deposits is marked by the presence of a thin layer of silty clay, called locally *caranto*, overconsolidated (OC) by a combination of desiccation and oxidation phenomena.

Concerning the classification and the index properties of the lagoon deposits, based on the mass of available information, in the following it is described a typical soil profile within the depth of 80m below m.s.l.. Silt and sand fractions are in the majority. On average at the MTS, the soil profile in the upper 60m is characterized by the presence of the following type of sediments: 35% sands (SP, SM<sup>1</sup>), 35% silts (ML<sup>1</sup>), 25% clays (CL<sup>1</sup>), 5% soils with relevant organic matter (MH, OH, Pt<sup>1</sup>). The mineralogical composition of sand and silt fractions can be alternatively siliceous or carbonatic. The latter contains detrital calcite and dolomite crystals and becomes more frequent with increasing the depth. The clay fraction is mainly composed of illite, muscovite with a slight presence of chlorite, kaolinite and smectite minerals. The liquid limit (LL) and plasticity index (PI) of the fine grained materials are generally within the following range; LL=36+/-9%, PI = 14+/-7%. Largely variable values of bulk density  $\gamma$  are generally in the range of 18.0 to 19.5 kN/m<sup>3</sup>. The in situ void ratio ( $e_0$ ), lies in the range of 0.60 to 0.85 except for organic materials where it is around 0.9 to 1.0, rarely exceeding 1.0. The sands are generally quite uniform but as the silt content increases the materials become growingly well graded.

On account of the above, Cola and Simonini (2002) made an attempt to correlate the strength and the deformation parameters of more coarse grained soils to an index coupling the mean normalized grain size ( $D_{50}$ ) with the uniformity coefficient  $U_c$ .

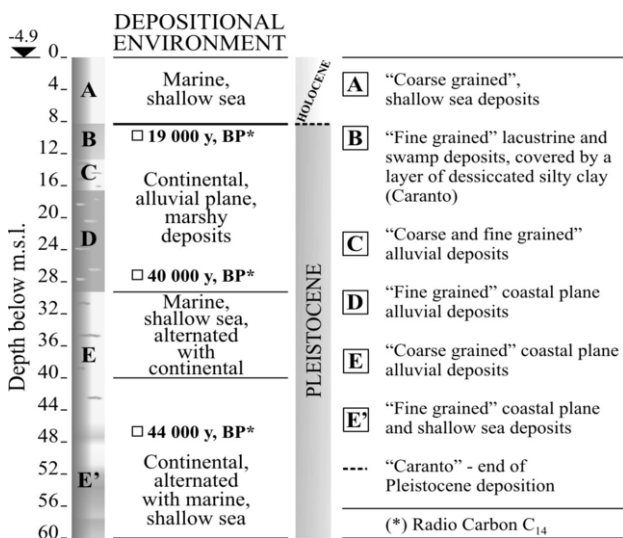


Figure 5. Scheme of depositional history at the Malamocco inlet (After Belloni and Caielli, 1997)

<sup>1</sup> According to Unified Soil Classification System

With regard to the compressibility and the deformation parameters obtained from laboratory tests, the following applies:

- The small strain ( $\epsilon_s < 10^{-3}$ ) shear modulus ( $G_0$ ) investigated by means of resonant column and bender element tests. Fig 6 shows the values normalized with respect to the mean consolidation stress ( $p'$ ) and the void ratio function  $f(e)$ , being  $p_a$  reference pressure equal to 100 kPa.
- The soil stiffness at higher strain levels has been inferred from the consolidated-drained triaxial compression (TX-CK<sub>0</sub>-CL) and extension (TX-CK<sub>0</sub>-EL) tests performed on fine grained materials; examples are shown in Fig 7a. The tests yield the values of the linear threshold strain  $3 \times 10^{-3} < (\epsilon_{ts}) < 6 \times 10^{-3}$ , see Leroueil & Hight (2002), depending on the overconsolidation ratio (OCR), PI, and on results generally higher in extension loading than in compression loading. Small unload-reload cycles have been applied in triaxial tests during the shearing stage to investigate the influence of shear strain ( $\epsilon_s$ ) on the unload-reload shear modulus  $G_{ur}$ . The obtained values are shown in Fig.7b and are compared against the secant  $G_s$  in Fig.7a.

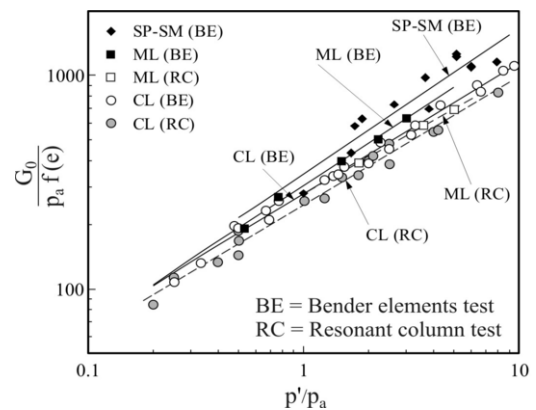


Figure 6. Normalized small strain shear modulus vs. normalized mean effective stress.

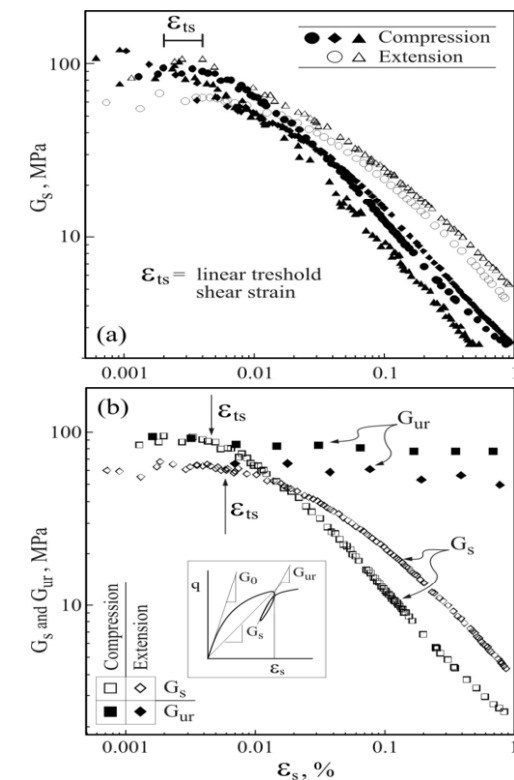


Figure 7. a) Secant shear modulus vs. shear strain b) comparison between secant shear modulus and unload-reload shear modulus.

The lagoon deposits compressibility was investigated via several oedometer tests. Their results are summarized in the following:

- Fig.8a reports some typical 1-D compression curves of silty clay (CL), silt (ML) and silty sand (SP, SM) materials. The tests have been interpreted for the following parameters
- Constrained modulus (M), Fig.8b shows the values of M versus vertical effective stress ( $\sigma'_v$ ) both normalized with respect to the reference stress  $p_a = 100$  kPa.
- Preconsolidation pressure ( $\sigma'_p$ ) corresponding in oedometer tests to the vertical yield stress ( $\sigma'_{vy}$ ). Because of the silty nature the soils under consideration exhibit a gradual transition from the recompression range to that of virgin compression, rendering the determination of  $\sigma'_p$  uncertain, but for the tests carried out on silty clay specimens.
- Consolidation coefficient ( $c_v$ ) of silty clays and silts obtained from the oedometer tests resulted in the range of  $10^{-5}$  to  $10^{-7}$  m<sup>2</sup>/s thus confirming the lagoon deposits trend to display high consolidation rates in the field conditions.

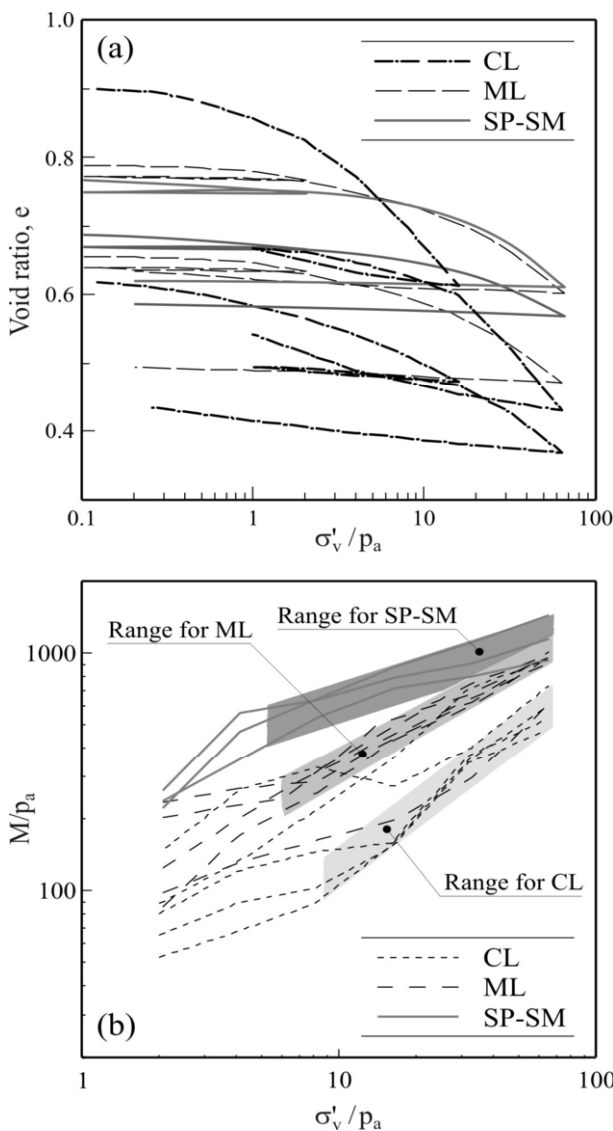


Figure 8. a) Examples of oedometer compression curves. b) Normalized constrained modulus vs. normalized vertical effective stress.

In Fig.9 it is shown the secondary compression coefficient  $C_{ae}$  for different lagoon soil types as function of  $\sigma'_v$ . The computed ratio of the primary compression index ( $C_c$ ) to  $C_{ae}$  ranges around 0.03 according to Mesri and Godlewski (1977) and Mesri et al (1995).

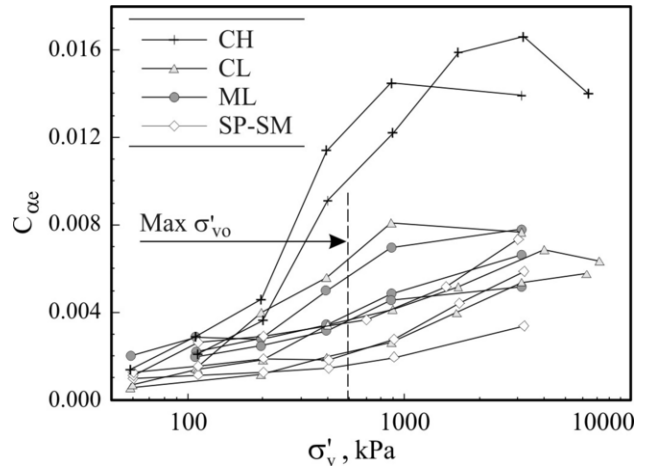


Figure 9. Coefficient of secondary compression vs. vertical effective stress at MTS.

As mentioned, the shear strength of the lagoon deposits was investigated by various triaxial tests whose results yielded the following information:

- Typically the lagoon sands and silts exhibit a dilative behaviour at failure. The contractive response at failure has been observed only for silty clays. Fig.10 reports the value of the maximum dilatancy rate at failure ( $d\varepsilon_v/d\varepsilon_1$ ) as function of mean effective stress at failure ( $p'_f$ ), where:  $\varepsilon_v$ = volumetric strain,  $\varepsilon_1$ =major principal strain. The shaded area includes the majority of the experimental results obtained for sands and silts. The data placed below the shaded area refer to soils containing a non negligible amount of clay fraction (CF) as pointed out in the figure itself.

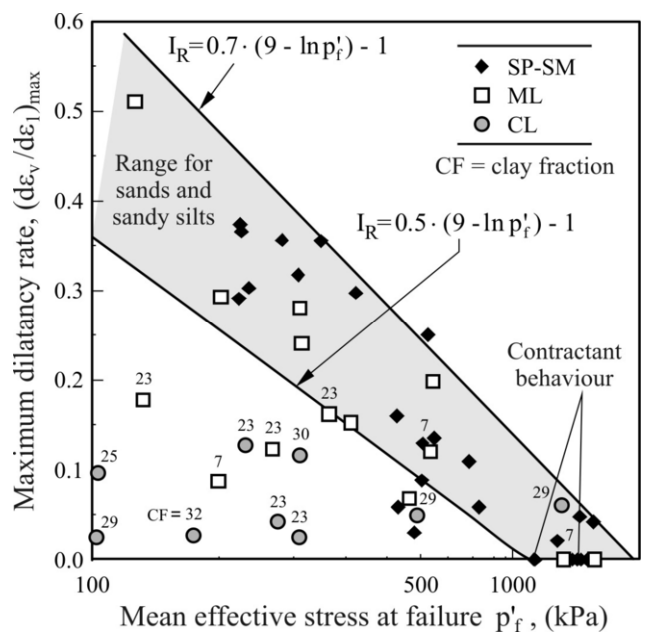


Figure 10. Maximum dilatancy rate vs. mean effective stress at failure.

As noted in Fig.10, the dilatancy vanished for sands and silts when the  $p'_f$  exceeds 1000-1200 kPa, in good agreement with the Bolton's (1986) simplified strength-dilatancy theory for sands, expressed by the equation:

$$(-d\varepsilon_v/d\varepsilon_1) = 0.3I_R \quad (1)$$

being:

$$I_r = D_R \cdot (Q \cdot \ln p'_f) - 1 \quad (2)$$

being:  $I_R$  = dilatancy index  
 $D_R$  = relative density  
 $Q$  = non dimensional parameter depending on the particles crushing strength.

Assuming  $Q = 9$  and taking into account the values of the maximum dilatancy rate measured for the  $p'_f$  of different magnitude, it is found the estimation of  $D_R$  between 50% and 70%.

- The values friction angle at critical state ( $\phi'_{cv}$ ) as inferred from triaxial compression tests resulted 33° to 39° and 30° to 34° for sands and silts respectively.
- The knowledge of  $\phi'_{cv}$  and of the peak angle of shearing resistance ( $\phi'_p$ ) resulting from triaxial tests, allows to estimate the state parameter ( $\psi$ ) [Wroth and Bassett (1965), Been and Jefferies (1985), Been et al. (1991)]. Fig.11 shows the dependence of  $\psi$  on the peak angle of shearing resistance ( $\phi'_p$ ) obtained via a relationship similar to that proposed by Wood et al (1994).

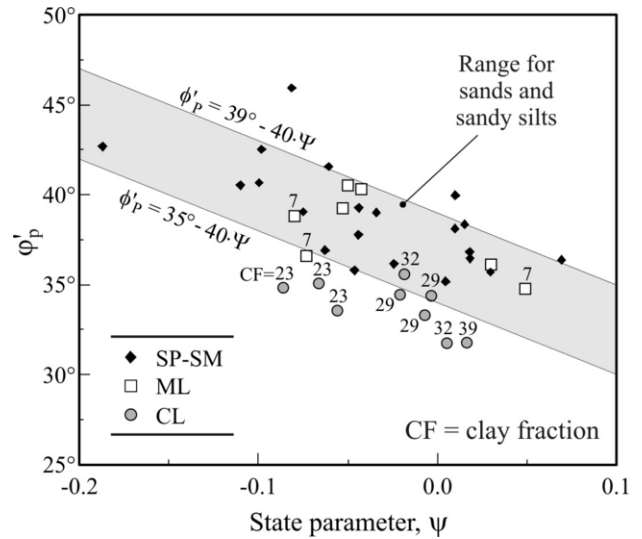


Figure 11. Peak angle of shearing resistance vs. state parameter.

On account of the MTS results and of the geotechnical exploration carried out for the final design (Fig.4), the geotechnical profiles have been drawn along the barriers axes, see Figs.12a through 12c. These figures, and principally, the displayed cone resistance profiles, prove the pronounced spatial variability of the lagoon deposits at the three inlets.

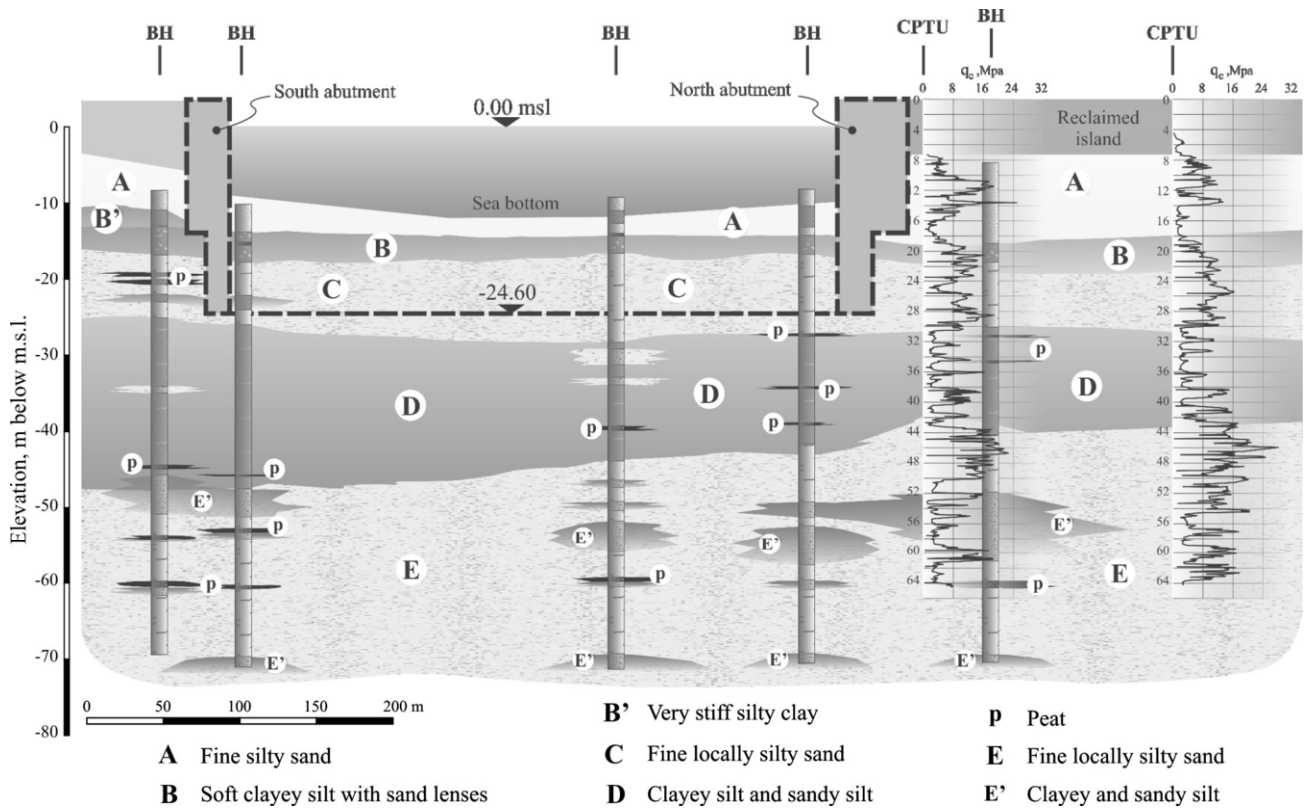


Figure 12a. Soil profile at the inlet of Lido-S.Nicolò.

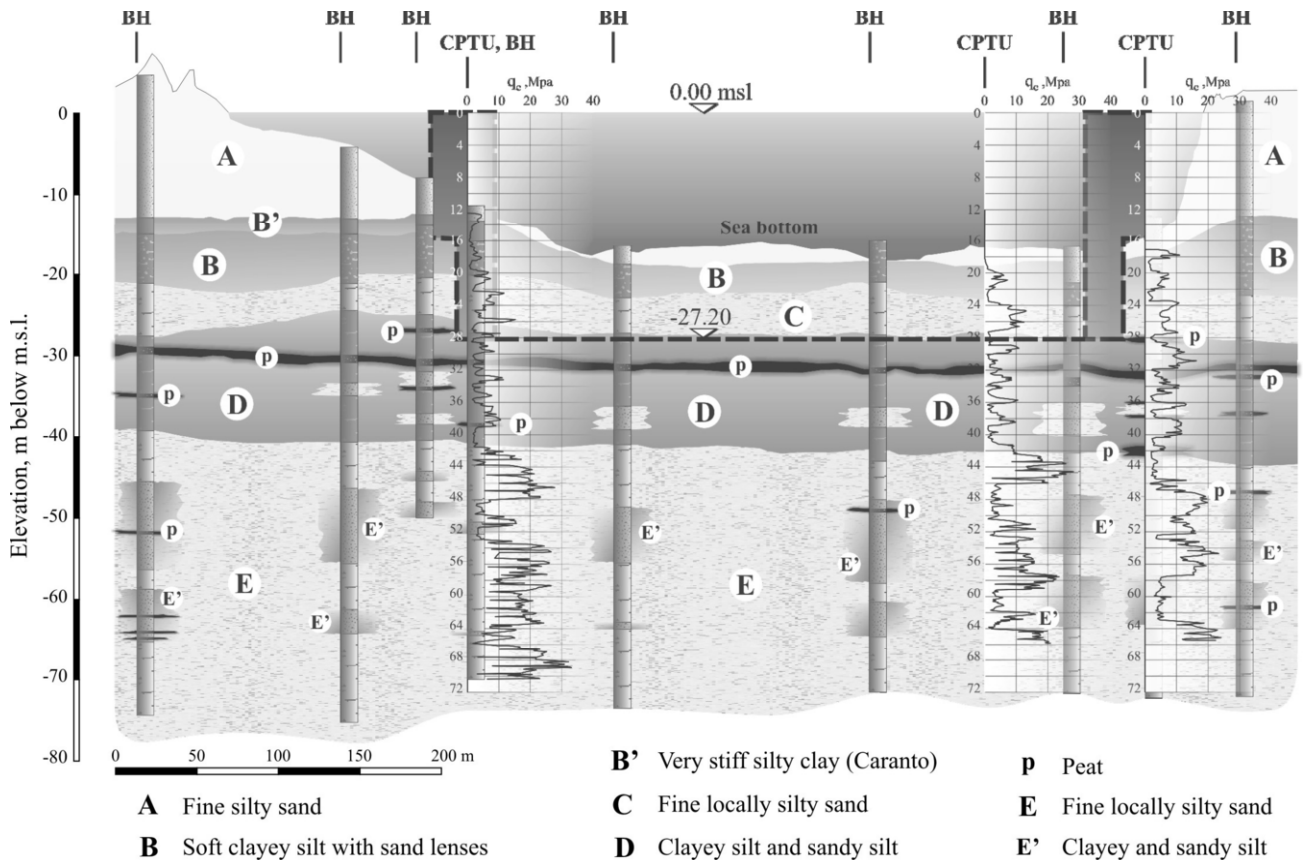


Figure 12b. Soil profile at the inlet of Malamocco.

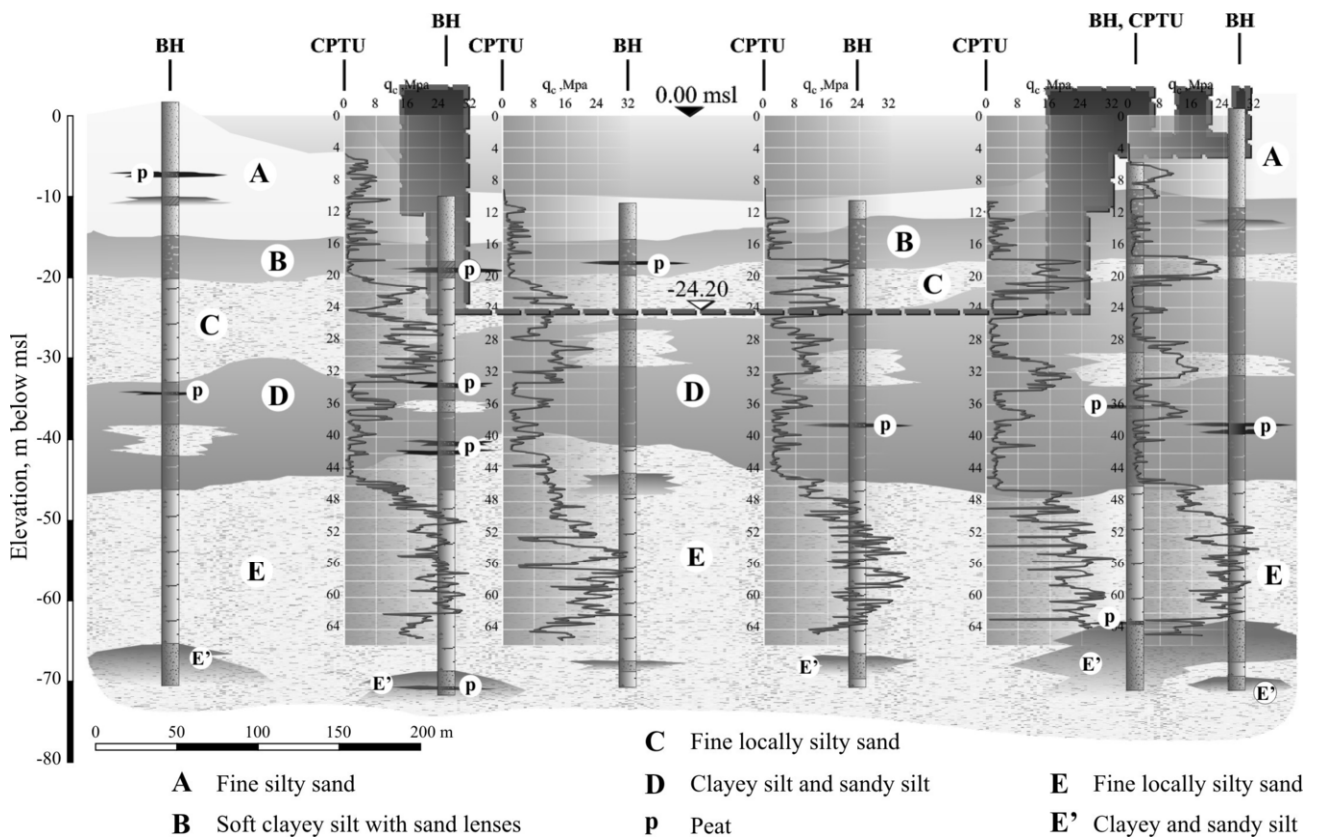


Figure 12c. Soil profile at the inlet of Chioggia.

To complete the site characterization, Fig.13 shows the  $V_s$  trend vs. depth as it emerges from all geophysical tests (CHT,S-DMT,S-CPTU) carried out at the lagoon inlets.

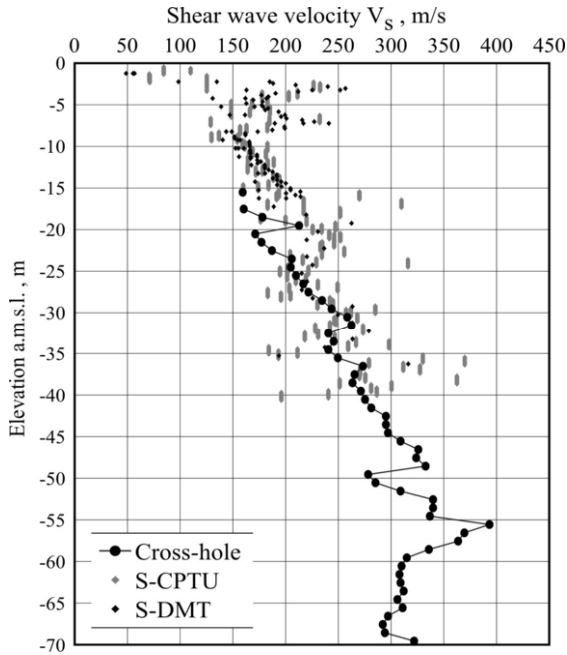


Figure 13. Shear wave velocity of the Lagoon deposits.

The CHT results have pointed out that at the lagoon deposit, to a considerable depth below the sea bottom, there are spots of not fully saturated soil, as supported by the CHT results carried at Malamocco site and reported in Fig.14. While  $V_s$  increases steadily with increasing depth, the  $V_p$  profile exhibits spikes of velocities lower than 1500 m/sec in the upper 30 m below the sea bottom suggesting the occurrence of unsaturated soils at depth.

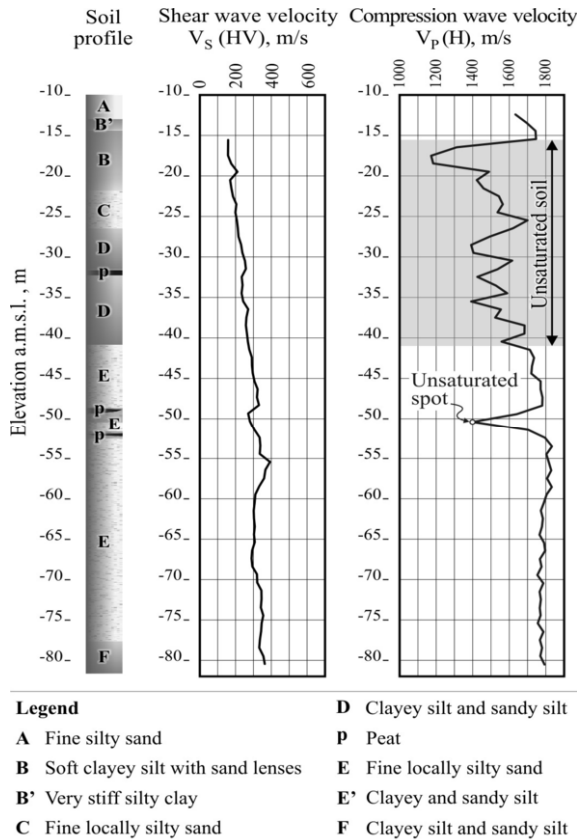


Figure 14. Results of cross-hole test at Malamocco inlet.

This is confirmed also by the response of the piezometers, embedded below the sea bottom, to high tides as reported in Fig. 15a, showing the range of the measured deamplification factor defined as ratio of the excess pore pressured measured at a given depth to tide elevation with respect to the m.s.l.. Moreover, Fig. 15b displays the values of the deamplification factor at four different elevations below m.s.l., corresponding to the piezometers location, computed for saturated and lightly unsaturated soils. This phenomenon can be ascribed to the presence of isolated gas bubbles at several spots of the lagoon deposits and confirms the experimental evidence that a deficiency in saturation as small as 0.5%, is enough to cause a significant drop of the  $V_p$  [Ishihara et al. (1998), Jamiolkowski (1999),Valle-Molina (2006)].

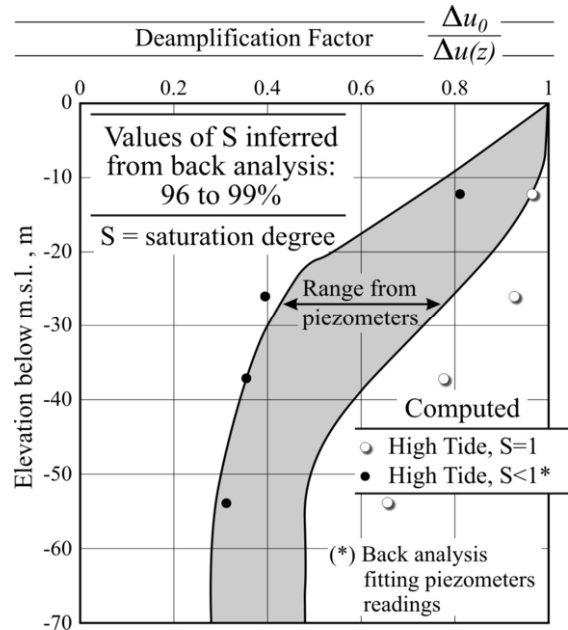


Figure 15a. Deamplification factor – Measured vs. computed.

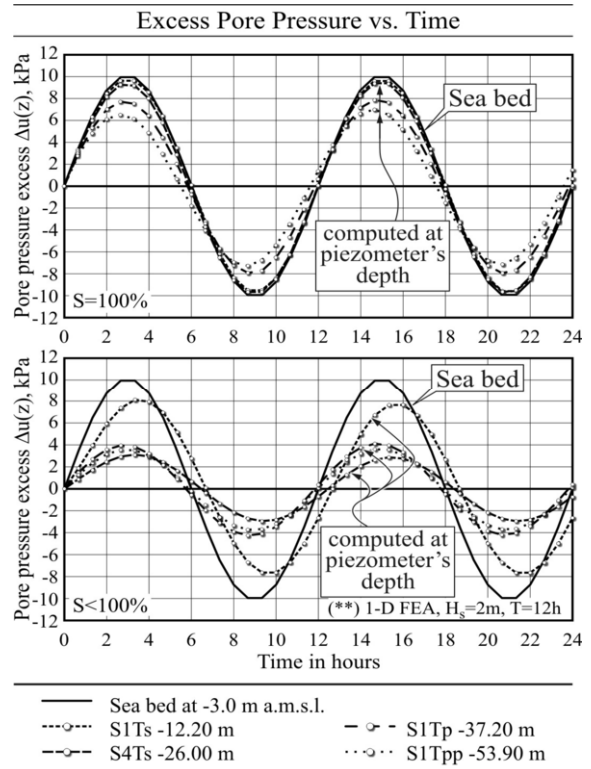


Figure 15b. Deamplification factor at the location of four piezometers.

Because of the intrinsic difficulties related to the spatial heterogeneity of the lagoon deposits and of the predominant presence of difficult to sample soils, it was decided to build up an instrumented trial embankment located at Lido-Treporti inlet to investigate the lagoon subsoil response to loading at large scale and to assess the relevant geotechnical design parameters accounting for the macrostructural feature of the deposits.

The task was assigned jointly to the Geotechnical Group of the University of Padova and the Consorzio Venezia Nuova. In the implementation of some in situ tests they involved the Universities of Aquila, Bologna and GeorgiaTech, Atlanta (USA). It was decided to build a 6.7m high, 40m in diameter vertically-walled circular sand embankment imposing around 107 kPa stress on the ground surface.

The site, referred in the following as the Treporti Testing Site (TTS), was thoroughly investigated, with undisturbed sampling, by means of in situ tests and borings [Marchetti et al. (2004), Gottardi & Tonni (2004), Mayne & Gillivray (2004)].

The soil characterization at the TTS yielded information concurring with those obtained at the MTS and from the geotechnical exploration carried out at the Lido and Malamocco inlets. Fig.16 summarizes grading, index properties and OCR profile at the TTS site.

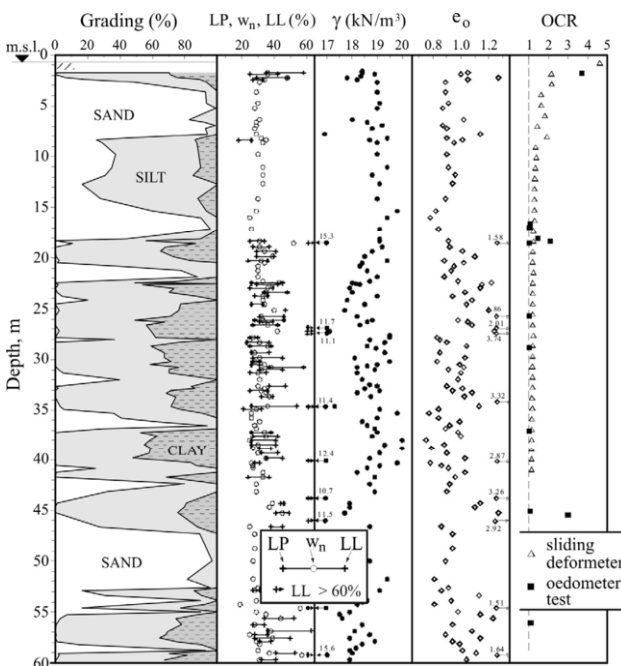


Figure 16. Soil profile and index properties at the TTS.

The corresponding soil profile extended to the depth of 55m can be summarized as follows:

- 1 to 3 m: soft silty clay, whose drainage has been improved by prefabricated drains
- 3 to 8 m: medium to fine silty sand;
- 8 to 20 m: clayey and sandy silt with a sand laminations encountered at depth between 15 and 18 m
- 20 to 22 m: medium-fine silty sand;
- 22 to 45 m: alternating layers of clayey and sandy silt;
- 45 to 55 m: medium-fine silty sand.

Based on the soil grading and on the index properties, the following geomaterials contribute to the soil profile within a depth of 55m: sands and slightly silty sands (SM + SP) 22%, sandy silts and silts (ML) 32%, inorganic silty clays (CL) 37% and organic clays + peat (CH+Pt) 9%.

Fig.17 reports the deformation parameters worked out from the oedometer tests performed on undisturbed samples retrieved from some borings carried out on TTS. The site characterization was highly enhanced by in situ tests whose results are summarized in Fig.18.

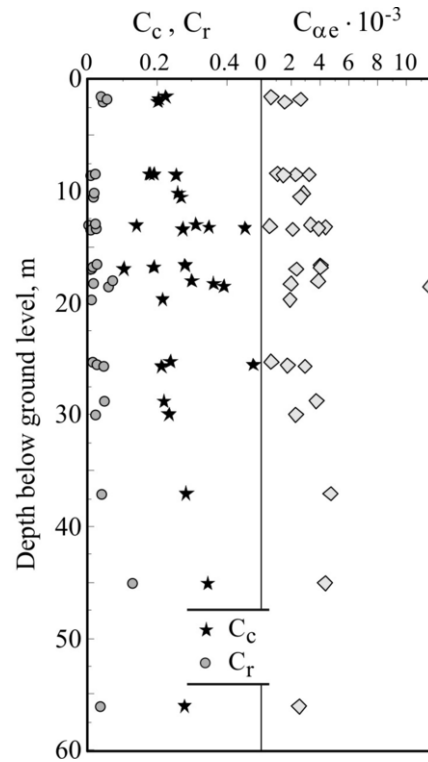


Figure 17. Compressibility parameters from oedometer test at the TTS.

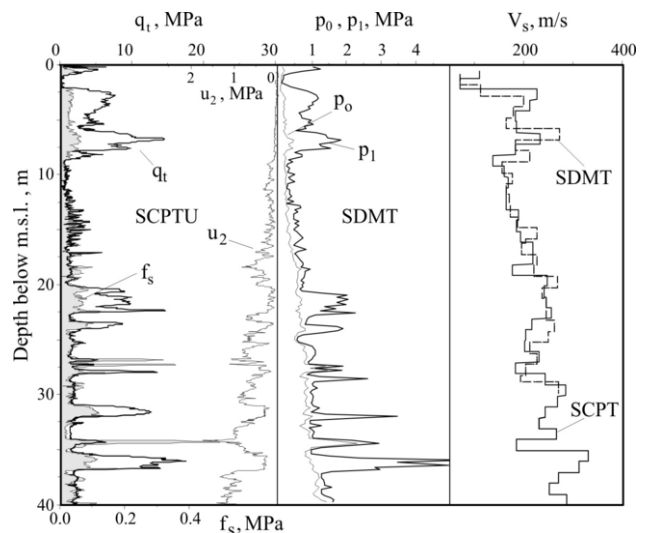


Figure 18. Example of in situ test results at the TTS.

The displayed results are similar to those yielded at other lagoon inlets confirming that the selected site can be representative for all the four barriers.

The trial embankment was completed in 2003 and removed in 2008. The picture of the cylindrical embankment, plan view and the cross-section, showing the monitoring instrumentation position, are illustrated in Figs.19a and 19b respectively and it can be inferred that the subsoil was heavily instrumented allowing to measure, in a redundant manner, the settlements as well as the horizontal displacements and the pore pressure during the whole trial life.

Special mention deserves the installation of four sliding deformers [Kovari and Amstad (1982)] allowing to measure the vertical displacement with depth at one-meter intervals with an accuracy of 0.03mm/m. These devices permitted to compute the vertical strain ( $\epsilon_v$ ) and its evolution at one-meter intervals achieving a deeper insight into the primary and secondary compression phenomena in situ.

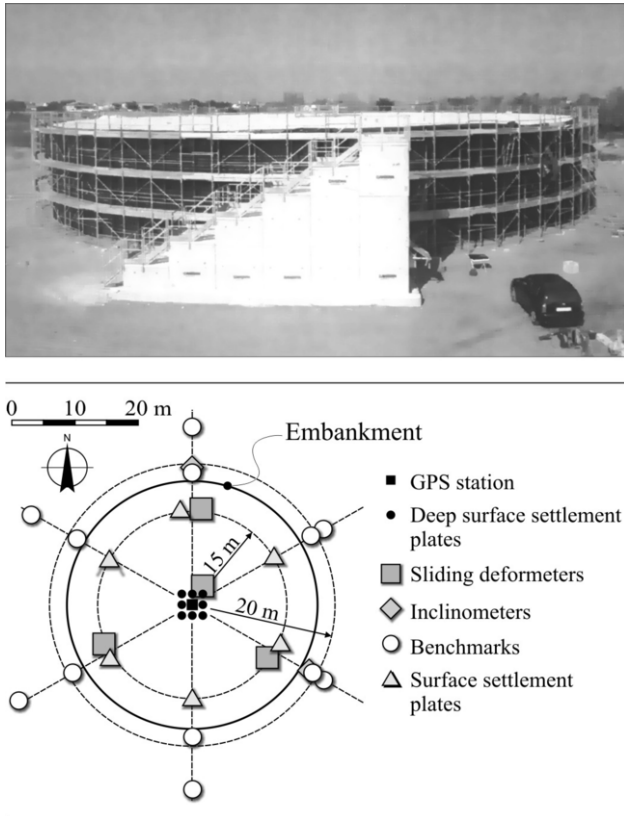


Figure 19a. Lido-Treporti trial embankment and layout of monitoring instrumentation.

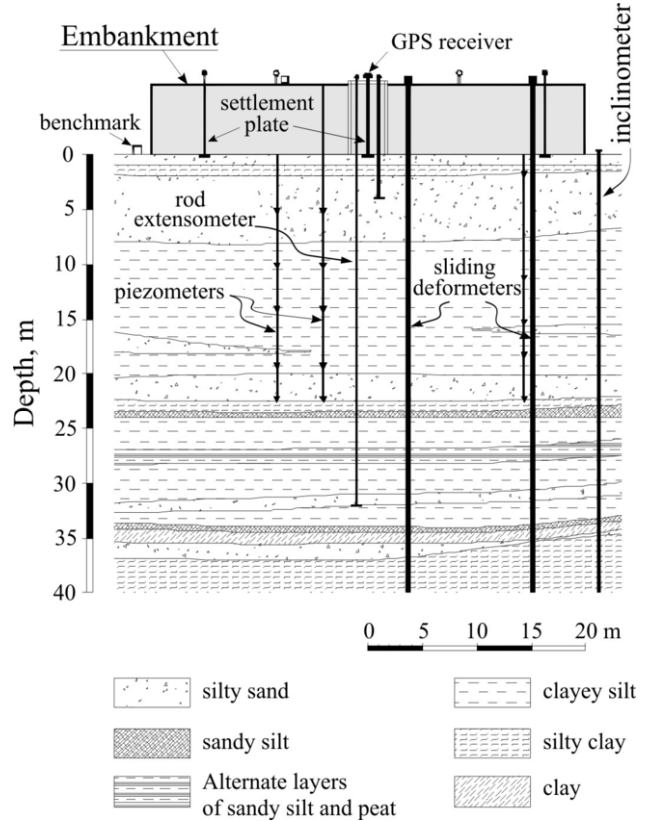


Figure 19b. Cross-section of trial embankment and underlying soil profile.

Fig.20 reports the construction history with the settlements measured under the trial embankment centre where the stress and the deformation condition replicate that of the 1-D compression. It is worth mentioning that the values of settlements measured by three independent methods during the entire 6-year monitoring period, to a large extent, yields coinciding results.

Going over this figure it can be assumed that during the embankment construction, occurred a nearly entire consolidation settlement. This circumstance is supported by the piezometers readings, not reported here, showing that at the construction end, the excess pore pressure was negligible and scarcely discernible from the sea level minor oscillations.

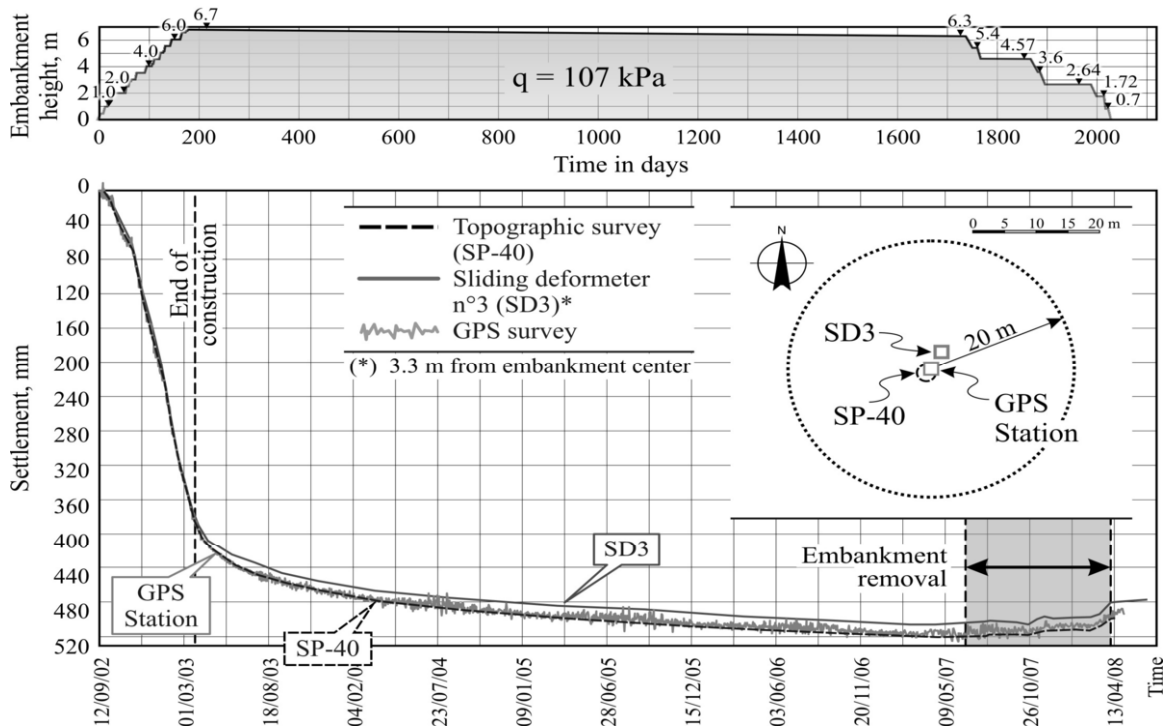


Figure 20. Time-settlement curves at the centre of the trial embankment, measured with different types of instruments.

Of outstanding value for understanding the response of the lagoon soil to the loading of large extension in plan, hence for the barriers design, are the distribution with depth of the vertical displacements and of  $\epsilon_v$  deduced from the sliding deformer located in the centre of the embankment given in Figs.21a and 21b respectively.

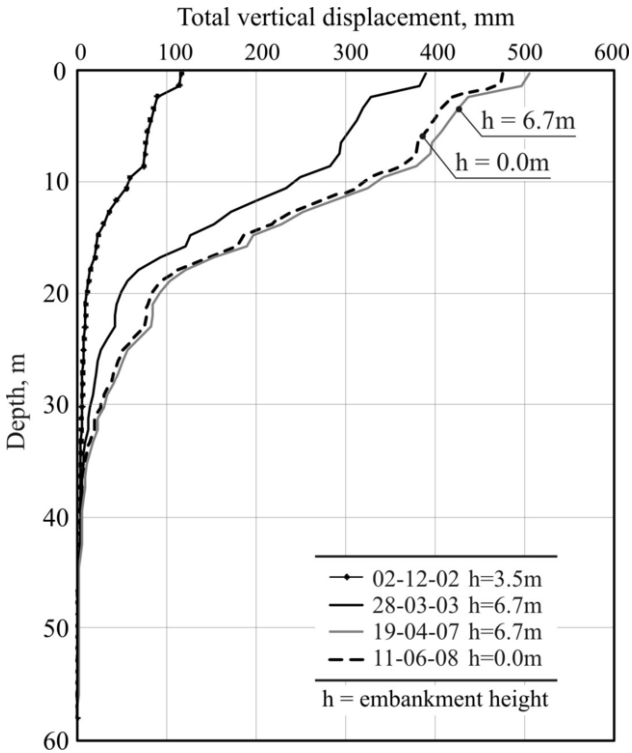


Figure 21a. Vertical displacement under the centre of trial embankment.

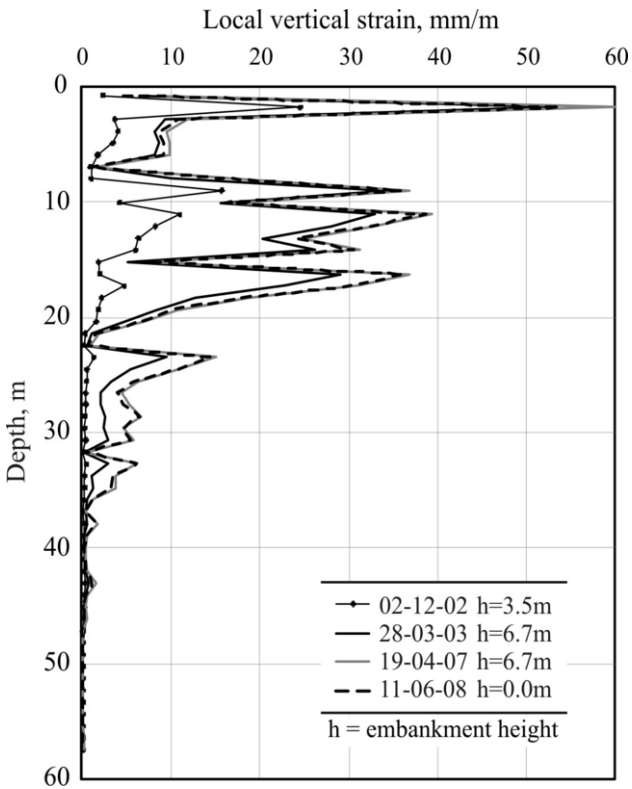


Figure 21b. Local strain under the centre of trial embankment.

These set of data made possible the construction of the field compression curves (Fig.22a) determining the trend of  $\sigma'_{vy}$  with depth thus, assessing the OCR profile shown in Fig.22b.

Benefitting of such plots, it was possible to compute for silts and silty clays the in situ constrained moduli  $M$  and compare them with those inferred from oedometer tests.

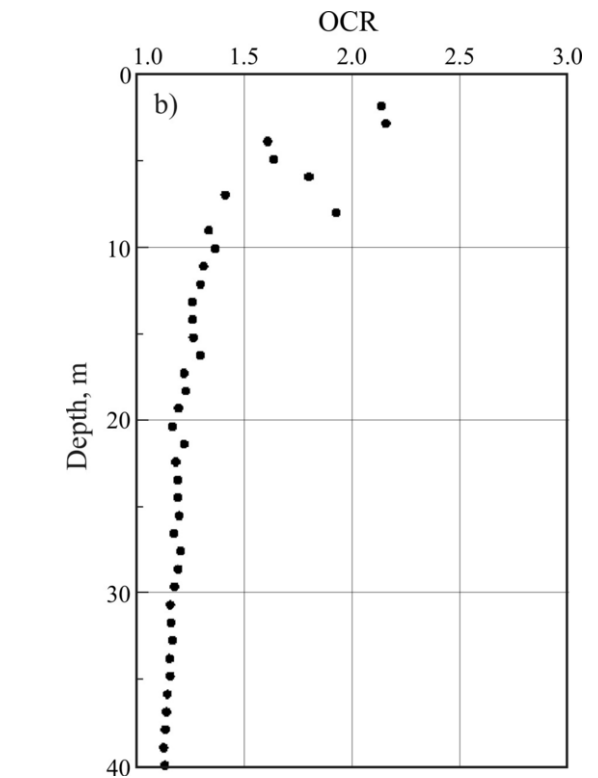
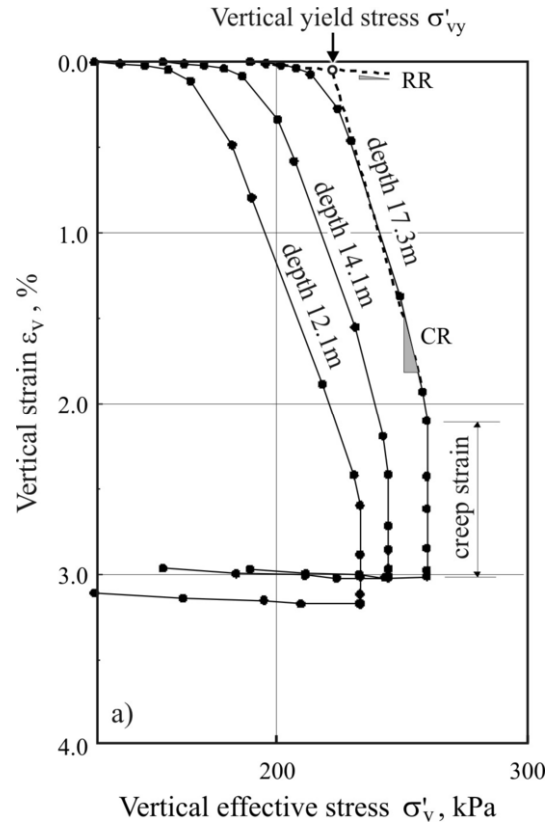


Figure 22. a) Field compression curves from sliding deformer. b) Overconsolidation ratio from field compression curves.

Fig.23 shows the results of this comparison, for the silty layer between 8 and 20 meters, extended to the unload M measured during embankment removal. As it should be expected the field values of M for  $\sigma'_{vo} < \sigma'_{vy}$  are appreciably higher than the laboratory determined values. The opposite is true when  $\sigma'_{vo}$  exceeds the  $\sigma'_{vy}$ . This experimental evidence can be attributed to the destructuration during sampling and laboratory testing to which the lagoon low activity silts and clayey silts are particularly prone.

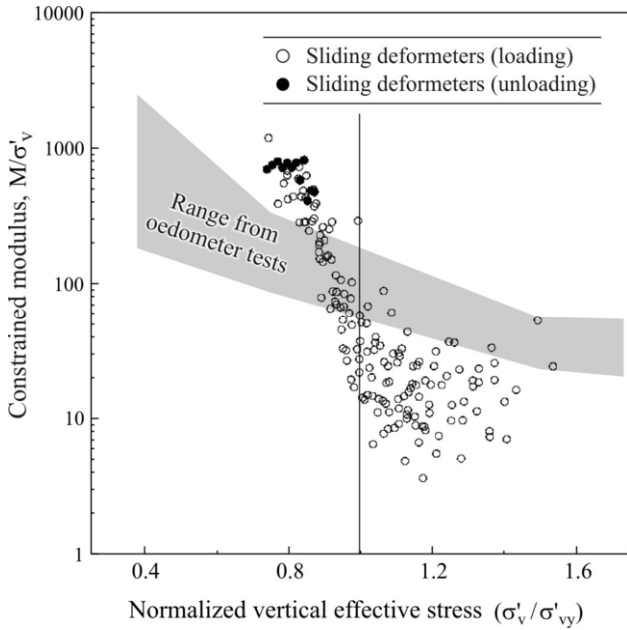


Figure 23. Site and laboratory normalized constrained modulus vs. normalized vertical effective stress.

The compressibility parameters RR (recompression ratio) and CR (compression ratio), are defined as follows:

$$RR = \frac{d \epsilon_v}{d \log_{10} \sigma'_v} \quad \text{for } \sigma'_v < \sigma'_{vy} \quad (3)$$

$$CR = \frac{d \epsilon_v}{d \log_{10} \sigma'_v} \quad \text{for } \sigma'_v > \sigma'_{vy} \quad (4)$$

Where,  $\sigma'_{vy}$  is the vertical yield stress.

A comparison of the RR and CR field and laboratory values suggests that:

- as it was to be expected, the ratio of RR (lab.) to RR (field) is appreciably higher than the unity, ranging between 1.5 and 2.5 for (SM+SP) soils and between 3.5 and 5 for (ML+CL) soils.

- For all the tested soils, the field values of CR are slightly higher than those determined in laboratory, indicating a moderate degree of destructuration of the undisturbed samples in the stress range beyond the vertical yield stress.

The secondary compression coefficient, as referred to the defined vertical strain ( $C_{\alpha\epsilon}$ ), may be evaluated from the field curves of  $\epsilon_v$  vs.  $\log_{10}$  time inferred from the sliding deformer readings. Examples of such curves are shown in Fig. 24. The comparison  $C_{\alpha\epsilon}$  (field) against  $C_{\alpha\epsilon}$  (lab), see Fig.25, by Simonini (2004) and Simonini et al. (2006) suggests that in fine grained soils the field values are, on average, 50% higher, while in coarse grained materials their ratio is near the unity.

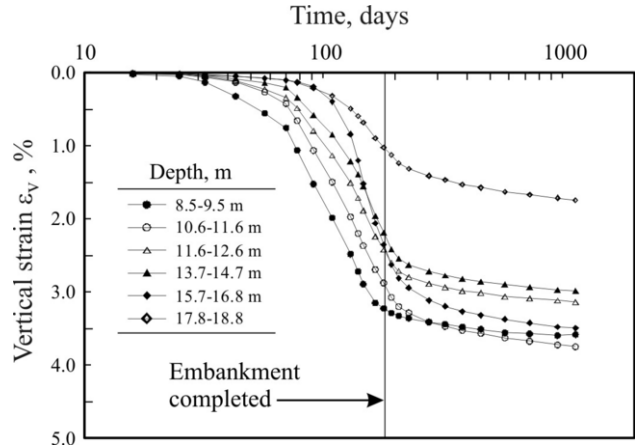


Figure 25. Vertical strain vs. time measured with the sliding deformer.

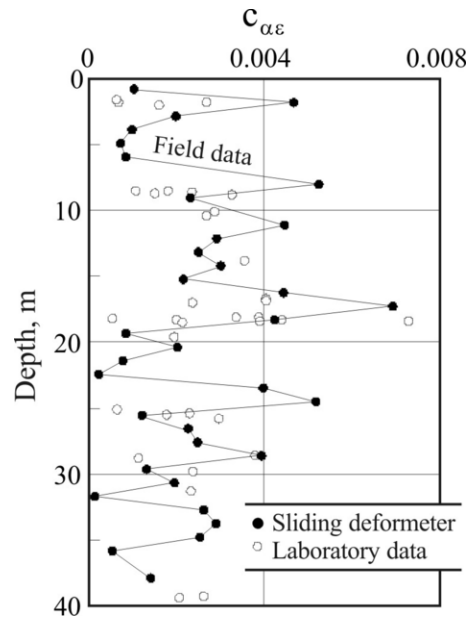


Figure 25. Comparison between field and laboratory secondary compression.

3 BARRIERS TO CLOSE THE LAGOON INLETS

The MOSE mobile barriers system, currently under construction, is the most important and challenging part of the interventions being implemented to safeguard Venice against high tide.

The MOSE System uses fold-away steel gates that are raised from the sea floor to prevent water from entering the Venice lagoon when high tide is forecast. It basically consists of four barriers, as shown in Fig. 3. The Lido inlet is 1.500 m wide and has been subdivided in two parts, Lido-Treporti and Lido-San Nicolò, by an artificial sand island in the middle.

The floodgates are normally folded and embodied in concrete caissons buried at the bottom of the lagoon inlets (Fig.26, upper part). In the occurrence of tides higher than +1.1 m, the mobile gates rise (Fig.26, lower part) isolating the lagoon from the Adriatic Sea for the limited lapse of time necessary to attain a drop of the sea level.

In the following is given, a detailed description of the San Nicolò Barrier (SNB) see Fig.27, with the aim to point up the noteworthy foundation problems and their solutions which, to a large extent, are similar for all the four barriers.

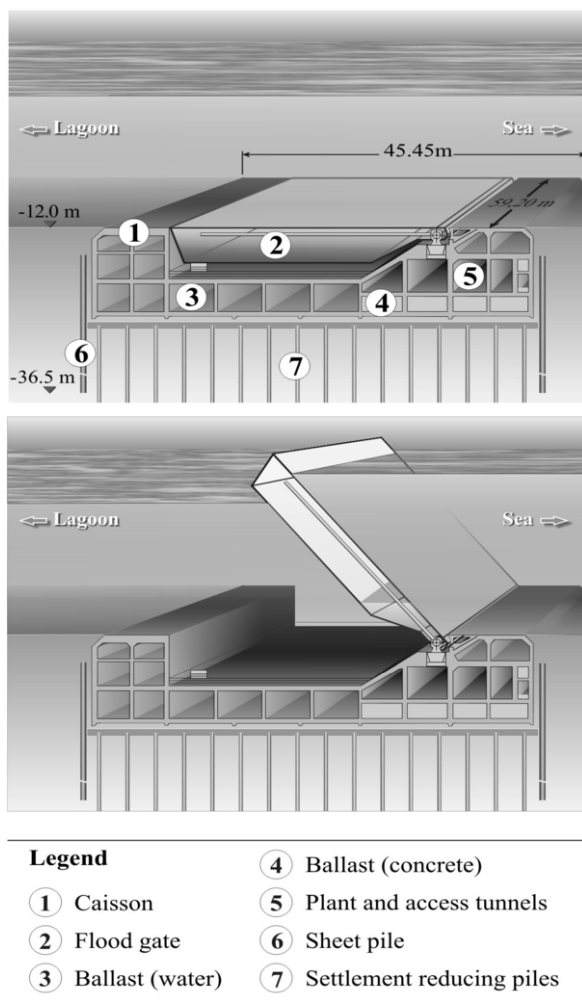


Figure 26. S.Nicolò barrier: flood gates operational scheme.

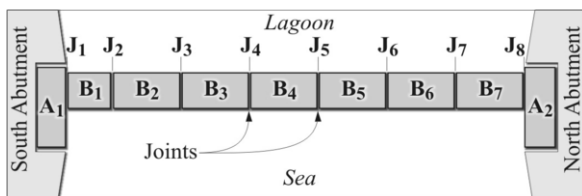
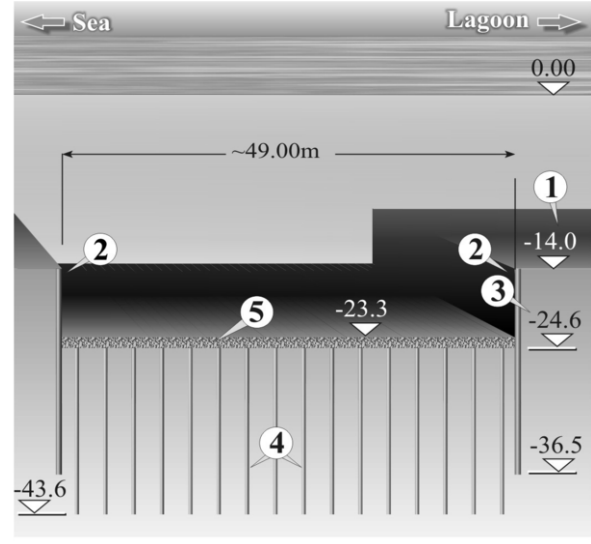


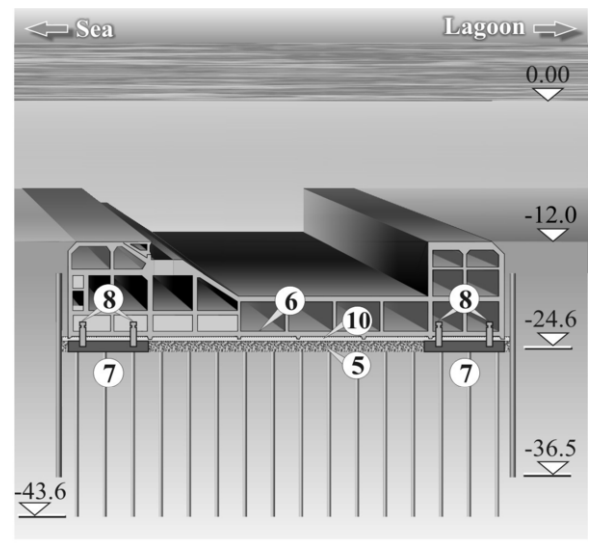
Figure 27. S.Nicolò barrier: plan view.

Fig.28 summarizes the SNB barrier construction as pictured in the design.

The geotechnical design of the barrier has posed countless challenges, however, only those related to the prediction of the caissons settlements, see Fig. 26 and Tab. 1, laying on settlement reducing piles will be presented here such as, the prediction of long term, up to 100 years, total and differential settlements under complex loadings accounting for self weight, tides and wave action as well as for low seismicity (PGA < 0.06g) earthquakes.



- ① Dredging to elev. -14.0 b.m.s.l.
- ② Sheet pile driving
- ③ Trench dredging to elev. -24.6 b.m.s.l.
- ④ Piles driving
- ⑤ Placement of granular fill 1.0 m, self levelling mortar 0.3 m



- ⑥ ⑦ Caisson placement on four temporary saddles
- ⑧ Levelling the caisson by means of hydraulic jacks
- ⑨ Caisson's ballasting
- ⑩ Grouting the space between caisson's bottom and granular fill

Figure 28. S.Nicolò barrier: construction sequence.

Table 1. Barriers of the MOSE system.

| Barrier location | Caissons n° * | Gates n° | Caissons dimensions, m                                     |          |          |
|------------------|---------------|----------|--|----------|----------|
|                  |               |          | length   | width    | height   |
| Lido - S. Nicolò | 9             | 20       | 40 to 60<br>each caisson incorporates<br>2 to 3 flap gates | 30 to 50 | 10 to 12 |
| Lido - Treporti  | 9             | 21       |  |          |          |
| Malamocco        | 7             | 19       |  |          |          |
| Chioggia         | 8             | 18       |  |          |          |

(\*) Does not include abutment caissons

- Time to open the gates: 30'
- Max water level difference: 2 m
- Time to close the gates: 15'
- Average closure time: 150'

Because of the barrier dimensions, of the complex construction sequence and of the pronounced subsoil spatial variability, a simplified approach to the settlement evaluation was selected and consisted in the following actions.

- The construction sequence including the caissons and the reclaiming fill placements were taken into account.
- The specific subsoil design profile under each caisson was considered.
- The stress increments in the subsoil were computed via the elasticity theory [Florin (1956)].
- The initial conditions to compute the settlements of the centre and of the four corners of the caissons were assessed based on the stress increments.

- The time-settlement behaviour of the fine grained soils was evaluated by a viscous-plastic coupled consolidation soil model [Zeevaert (1972), Rocchi et al. (2003)] adapted to the conditions of one-dimensional compression.
- The settlement of coarse grained soils was computed assuming a fully drained loading and adopting the elasto-plastic strain hardening model [Li & Dafalias (2000)].

In Appendix A the soil parameters used in the settlement calculations are detailed. They have been obtained from laboratory tests, seismic in situ tests and from back analyses of the instrumented trial embankment, previously considered.

The deformation modulus within the depth of the soil treated with the settlement reducing piles was assessed using the homogenization approach. Because of the variability of the design soil profile along the axis of SNB, the equivalent deformation modulus varies in a wide range between a minimum of 32 MPa under caisson n. 2 to a maximum of 82 MPa in correspondence of the North abutment caisson.

The predicted settlements at different occasions, after the end of construction, are shown in Fig. 29. The relevant differential displacements and rotations of caissons nn°1, 2 and 9 (Fig.27) alongside the abutments are due to the settlement induced by the reclaimed sand fill to be placed behind the abutment caissons and, as such, dependent on the temporal construction sequence considered in the calculation.

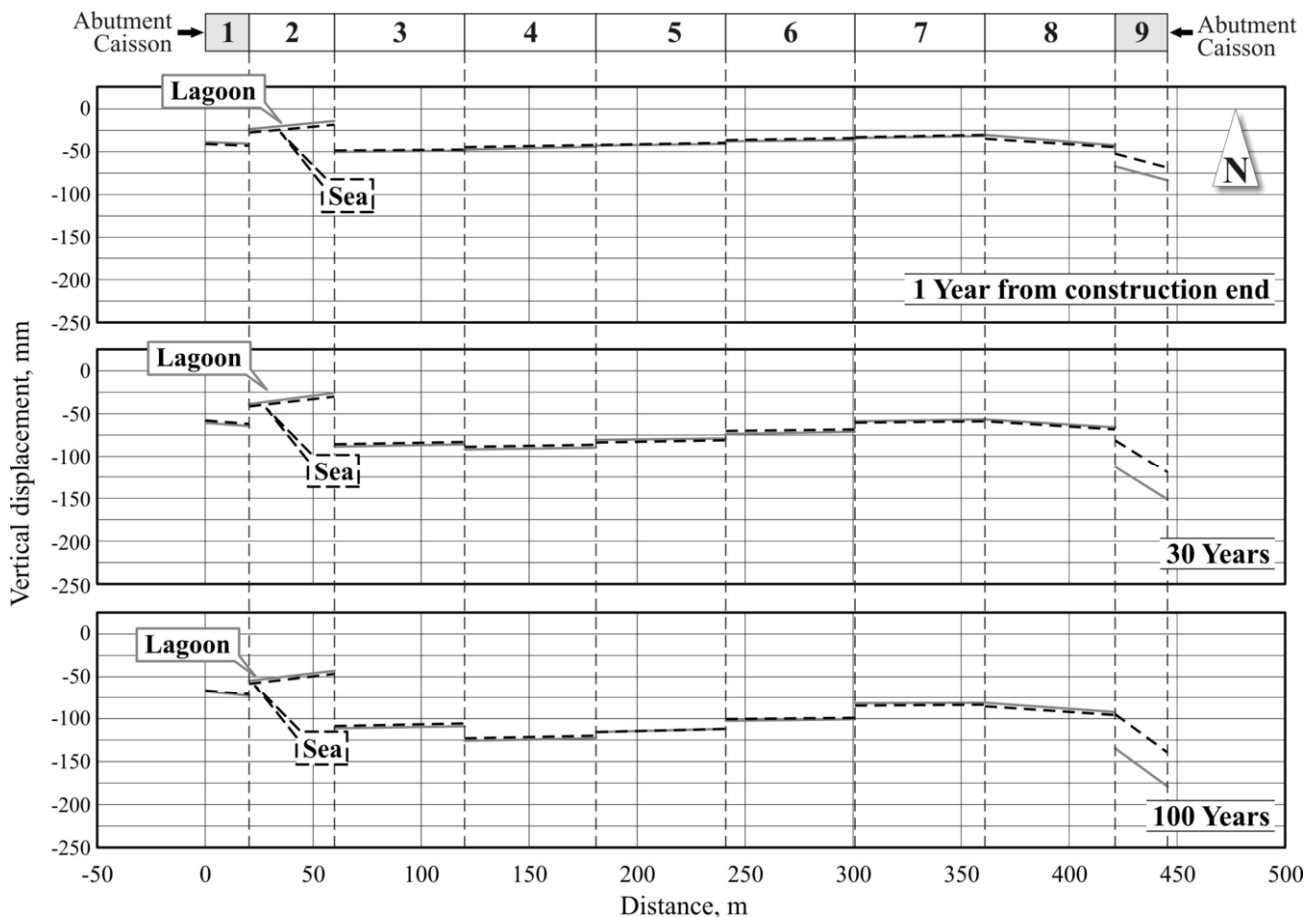


Figure 29. Computed vertical displacements of caissons of the barrier at S.Nicolò inlet.

Special attention was paid to the analysis of differential settlements, regarded as the most crucial aspect in geotechnical design. Fig. 30 shows the cross section of a generic caisson perpendicular to the barrier axis, with a number of large rubber joints, which provide a waterproof contact between two adjacent caissons, thus guaranteeing accessibility of the service tunnels for the maintenance of the electro-mechanical equipments operating the mobile gates.

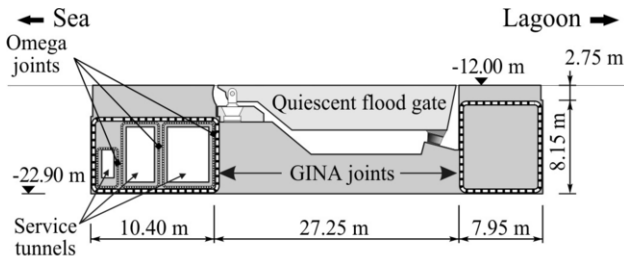


Figure 30. Cross-section of a caisson with the layout of the waterproofing joints.

The joints integrity requires that the maximum differential settlements between two contiguous caissons should not exceed the values exposed in Tab.2, being:

- $\Delta_1$  = differential vertical displacement of two adjacent caissons, Fig. 31a;
- $\Delta_2$  = rotation of two contiguous caissons causing the compression/decompression of Gina/Omega joints, Fig. 31b;
- $\Delta_3$  = change in horizontal distance between the flood gates housed in two adjacent caissons, Fig. 31c

Figures 31a through 31c describe the conventional signs adopted in the definition of the  $\Delta$  values.

The computed maximum differential displacements at locations of SNB joints (Fig. 27) are shown in Tab.3. The values yielded by the calculations are generally well below the acceptable limits with the exception of the two abutment caissons and the barrier caissons 6 contiguous to the abutments.

Table 2. S.Nicolò barrier: maximum tolerable differential displacements (including construction imperfections).

| Joint | Joint n°<br>(See fig.27)          | $\Delta_1$<br>mm | $\Delta_2$<br>mm | $\Delta_3$<br>mm                   |
|-------|-----------------------------------|------------------|------------------|------------------------------------|
| GINA  | J <sub>2</sub> to J <sub>7</sub>  | ± 40             | +29              | 124                                |
|       | J <sub>1</sub> and J <sub>8</sub> | ± 40             | +33              | 127                                |
| OMEGA | J <sub>2</sub> to J <sub>7</sub>  | ± 40             | +40              | Distance<br>between<br>flood gates |
|       | J <sub>1</sub> and J <sub>8</sub> | ± 40             | +40              |                                    |

Table 3. Maximum values of computed differential displacements.

| Joint n°       | $\Delta_1$<br>mm | $\Delta_2$<br>mm | $\Delta_3$<br>mm |
|----------------|------------------|------------------|------------------|
| J <sub>1</sub> | 17 (30y)         | <5               | 7 (100y)         |
| J <sub>2</sub> | 55 (100y)        | <5               | <5               |
| J <sub>3</sub> | -15 (100y)       | <5               | <5               |
| J <sub>4</sub> | -8 (EOC*)        | <5               | <5               |
| J <sub>5</sub> | 11 (100y)        | <5               | <5               |
| J <sub>6</sub> | 17 (100y)        | <5               | <5               |
| J <sub>7</sub> | -9 (EOC*)        | <5               | 7 (EOC*)         |
| J <sub>8</sub> | -19 (30y)        | 15 (100y)        | 51 (100y)        |

(\*) EOC: End of construction

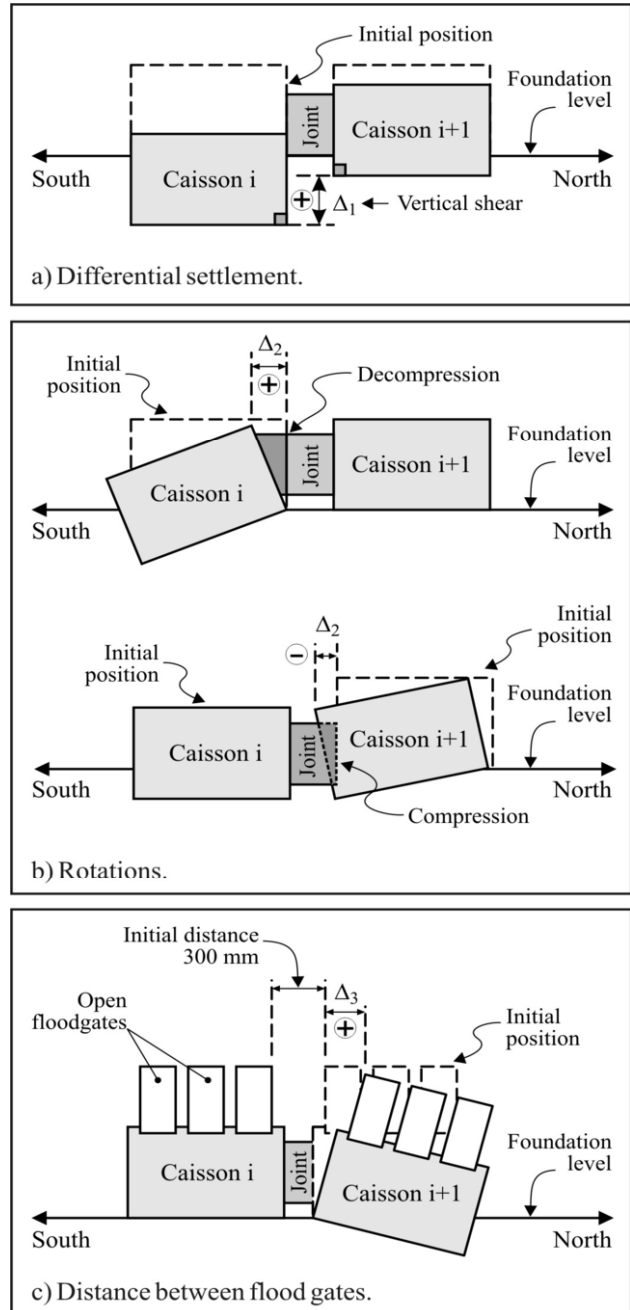


Figure 31. Differential displacements accounted in design.

The larger differential settlements at these spots are induced by the placement of reclaiming fill behind the abutment caissons and by the construction of the artificial island which splits the Lido inlet in two parts (Fig. 3). The computed differential settlement adopted in the analysis is, to a large extent, controlled by the construction sequence and by the time elapsing between the end of reclamation works and the placement of the caissons.

Such sequence can be modified, if necessary, to mitigate the impact of differential displacements at the critical locations.

The caissons lay on 500mm in diameter 19m long spun driven concrete piles. The piles will be driven after dredging, between sheet piles (Fig.28), the inlet bottom to elevation -24.6. below m.s.l. Then the piles head will be covered by 1m compacted granular fill and 300mm of self-levelling mortar to obtain an evenly distributed contact under the caisson slab.

In the preliminary design stage, in early 1980s, the piles were meant to mitigate the differential settlement due to the spatial soil variability and to any possible construction imperfections linked to the complexity of underwater works.

The current awareness of the piled foundation design principles allows asserting that the piles act as settlement reducers [Burland (1990), Viggiani (1998), Viggiani (2001)].

The mechanism of the load sharing between the piles and the surrounding ground was analyzed using the code NAPRA [Russo (1998), Mandolini et al., (2005)].

The code essential features can be summarized in following:

- Stratified linear elastic half space
- Variable raft stiffness
- Variable piles geometry and material properties
- Tensionless raft-soil contact
- Interaction at the raft-pile contact, non-linear elastic.
- Interaction among piles, linear-elastic assuming a cut-off at the distance  $r_m$  as suggested by Randolph and Wroth (1978)
- Piles connected to raft by hinges

The analysis carried out by NAPRA for one of the standard SNB caisson are exposed in Fig. 32 which reports two basic information steering the design of rigid raft on settlement reducing piles:

$$\alpha_p = \frac{\text{Vertical load on piles}}{\text{Total vertical load}} \quad (5)$$

$$\alpha_s = \frac{\text{Settlement of piled foundation}}{\text{Settlement of unpiled foundation}} \quad (6)$$

Accounting for the mentioned restrictions imposed on the barriers differential settlements, it was determined to adopt a spacing between piles equal to 3.8 m. With such spacing, referring to the total acting permanent load of 158626 kN corresponding to the total number of 268 piles, one gets,  $\alpha_p=0.72$  and  $\alpha_s=0.61$ . The loads on piles in different operational conditions are shown on Tab.4.

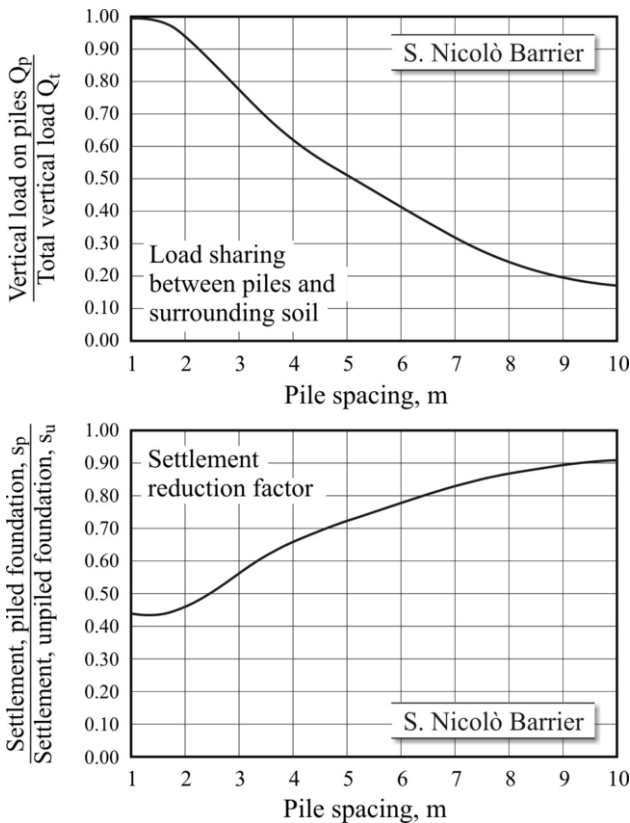


Figure 32. Results of soil-structure interaction analysis carried out by the code NAPRA, Russo (1998).

Table 4. Load on piles.

| Loading conditions  | $(Q_p)_{max}$ kN | $(Q_p)_{min}$ kN | $(Q_p)_{av}$ kN | $\Sigma Q_p / Q_t$ % |
|---------------------|------------------|------------------|-----------------|----------------------|
| Quiescent floodgate | 725              | 535              | 614             | 66                   |
| Floodgate open      | 793              | 520              | 642             | 65                   |

$Q_p$  = load on a single pile,  $Q_t$  = total vertical load.

The NAPRA code was validated by means of a comprehensive series of centrifuge tests carried out at ISMGEO [Fioravante et al. (2007)] and by finite element analyses [Bonizzoni and Daprat(2006)] performed using the TOCHNOG code, (1989) carried out using the same visco-plastic constitutive model adopted in the evaluation of the barrier settlement. Both physical and numerical modelling confirm the response of NAPRA both in terms of load sharing mechanism ( $\alpha_p$ ) and of settlement reduction factor ( $\alpha_s$ ).

Moreover, the physical and numerical modelling show that the placement of a granular layer between the caisson bottom and the piles heads generates a negative shaft friction over almost the upper half length of the piles, see Figs. 33 and 34.

The phenomenon can be attributed to the circumstance that the insertion of a deformable layer between the caisson's slab and the piles head inhibits the effective displacement compatibility between the raft and the piles.

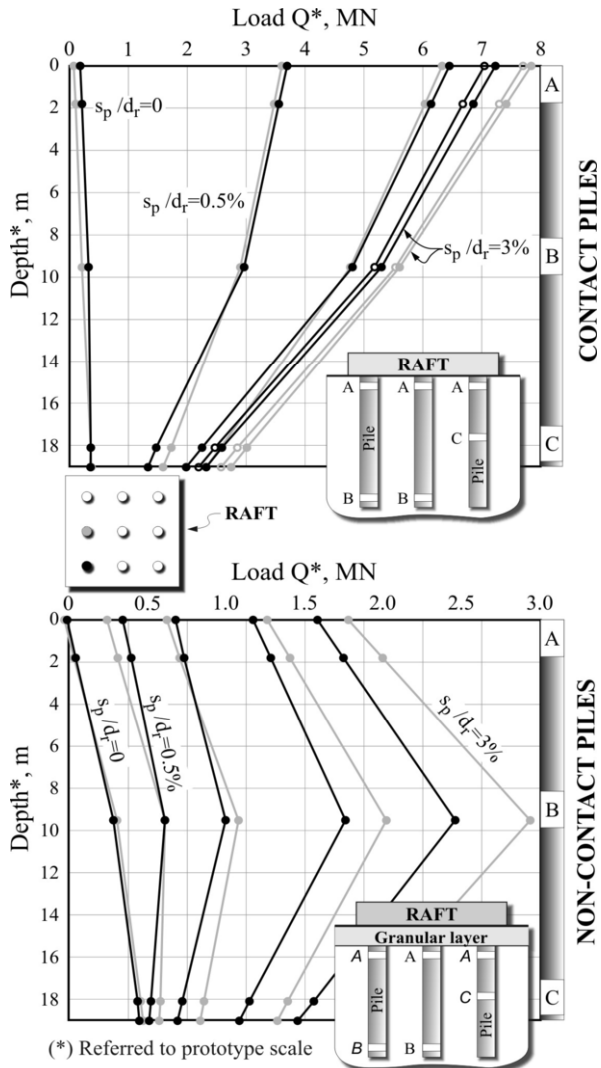


Figure 33. Square raft with nine piles on silty sand: axial load distribution along piles from centrifuge tests. ( $d_r$  = raft diameter) Fioravante et al. (2007).

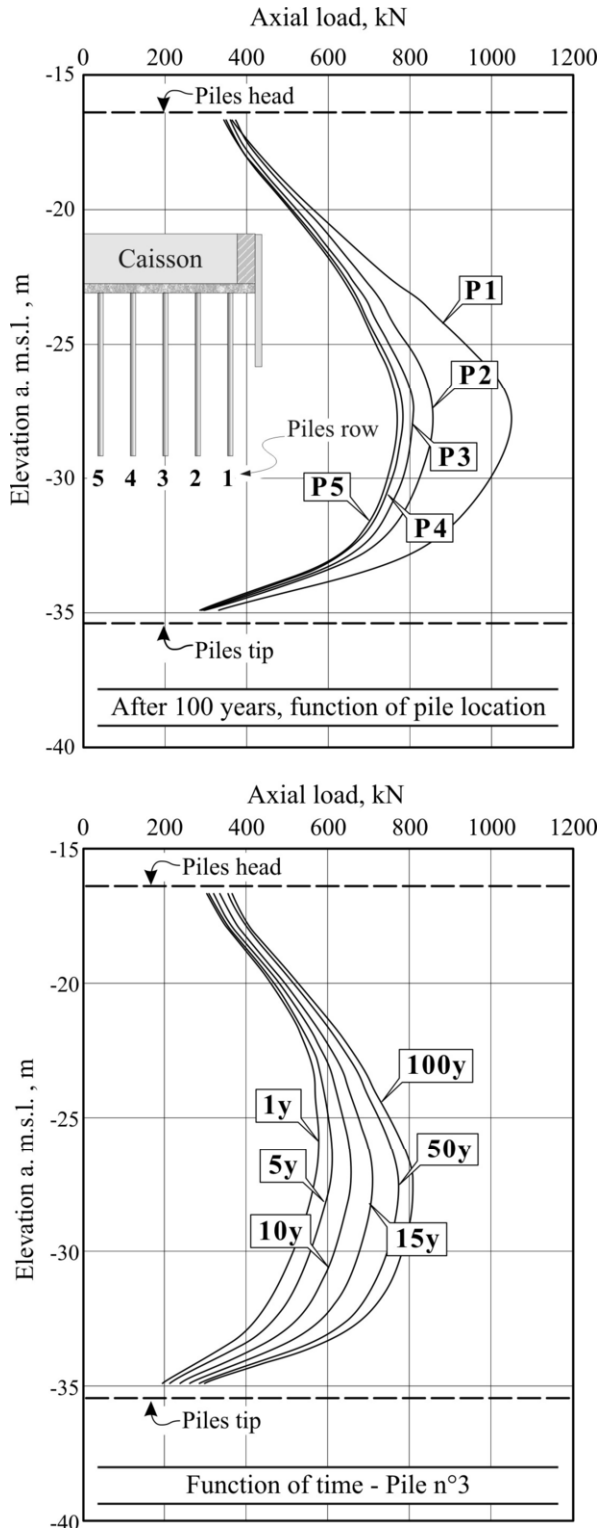


Figure 34. Load distribution along piles from F.E. analysis. Bonizzoni and Daprat (2006).

#### 4 SUMMING-UP

The overall scheme for the safeguard of Venice from flooding has been briefly illustrated, focusing on two specific items.

Safeguarding Venice and other settlements inside the lagoon against exceptionally high tides exceeding the elevation +1.1 m m.s.l. by means of barriers housing mobile gates capable to close temporarily the inlet into the lagoon.

Local interventions aimed at avoiding flooding of some limited areas of the city during tides exceeding +0.8 m m.s.l. Many local interventions have been designed aimed at avoiding flooding of a limited area of the city during tides exceeding elev. +0.8 m.s.l. and some of them have been implemented. A relevant example is the design conceived to waterproof the most valuable San Marco Square, as illustrated in the work by Burghignoli et al. (2007).

The design and the implementation of the planned interventions aroused quite a number of unique challenge demands to geotechnical engineers because of the difficult geotechnical and environmental conditions. Among them:

- The complex depositional environment, responsible for the pronounced spatial variability of the lagoon deposits, rendered the site characterization a challenging task. In the circumstances, the in situ tests, especially the geophysical one, geotechnically-oriented, have played quite a relevant role.
- The interpretation of information yielded by the large scale, heavily instrumented, embankment, step of paramount importance in the geotechnical design.
- The need for predicting the long term settlements of the barrier caissons over a period of 100 years, owing to the tight limitation of differential settlements. Secondary compression, ratcheting caused by waves and tides as well as placement of the reclaimed fills in the vicinity of the barriers have been considered in the prediction.
- The complex sequence of construction and the related issues regarding quality control and assurance during the execution of the foundation works.

As to the project advancement, many complementary interventions have been already completed.

The prefabrication of the barriers caissons was started in Spring 2008 and in the summer the project advancement had reached approximately 50%, its completion is scheduled in 2013.

APPENDIX A: SOIL MODELS EMPLOYED IN SETTLEMENTS CALCULATIONS

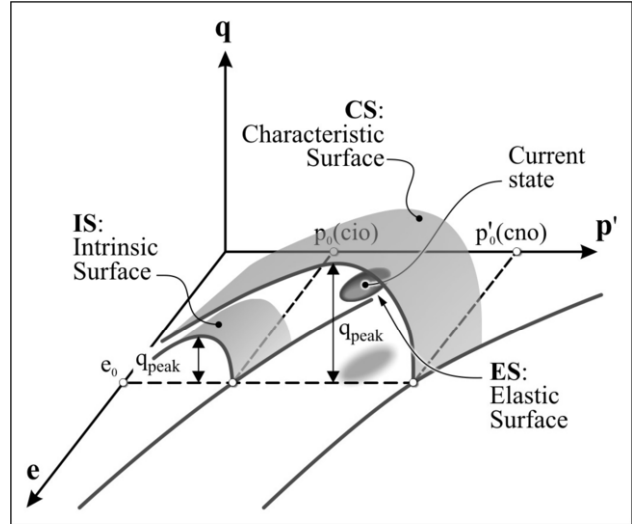
The long term settlements prediction was computed following the simplified procedure summarized in Section 3.

In the fine grained, predominantly silty materials (strata B, D, E and F, Fig.A-1), an elastic-viscous-plastic constitutive model (VISCO-CLAY) have been employed (Rocchi et al. 2005) which works along the lines of the framework developed by Rocchi et al (2003). In the void ratio (*e*), the deviator stress (*q*) and the mean effective stress (*p'*) space, the VISCO-CLAY adopts two limit surfaces (see Fig.A-2):

-Inner, Intrinsic Surface (IS), inside which the viscous phenomena are inhibited.

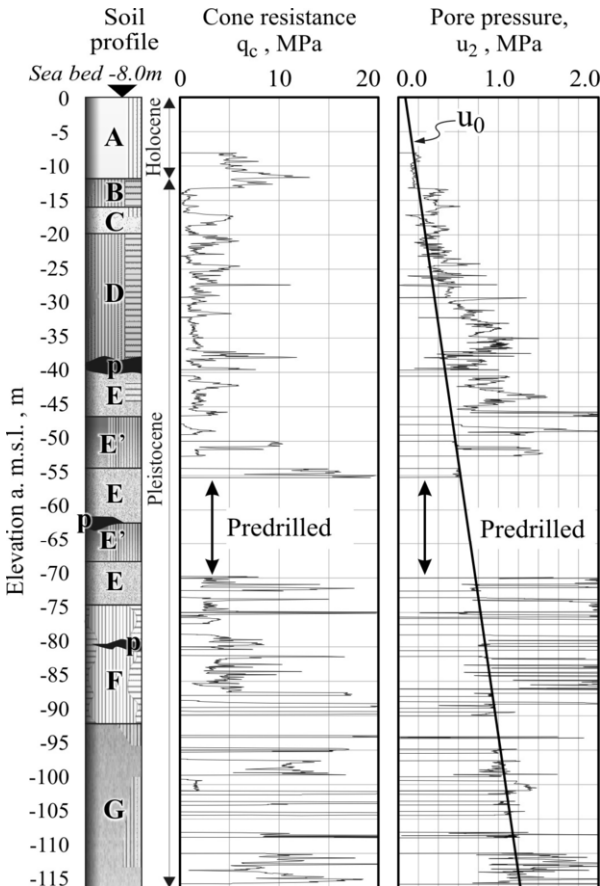
-External, Characteristic Surface (CS), which depends on depositional and post-depositional phenomena processes experienced by the material. A viscous phenomena can arise when the current state of the material is located inside and at this surface. The viscous phenomena are activated when the current state exceeds an elastic yield locus defined around the initial material state.

The shape of the IS and CS surfaces is the same used for Cam-Clay Models (CCM) family. The dimension is governed by the isotropic effective stress  $p'_{cn}$  (for the CS) and  $p'_{ci}$  (for the IS). The initial value of  $p'_{cno}$  (Fig.A-2) is linked to the value of the vertical effective yield stress  $\sigma'_{vy}$ .



**q** = deviator stress      Inside ES:  $\epsilon_t = \epsilon_e$   
**p'** = mean effective stress      Inside IS:  $\epsilon_t = \epsilon_e + \epsilon_p$   
**e** = void ratio      between IS and CS:  $\epsilon_t = \epsilon_e + \epsilon_p + \epsilon_{vi}$

Figure A-2. Constitutive model adopted for fine grained soils – Rocchi et al. (2003, 2005).



| Legend |                                  |
|--------|----------------------------------|
| A      | Fine silty sand                  |
| B      | Clayey silt with sand lenses     |
| C      | Fine, locally silty sand         |
| D      | Clayey silt, seems of sandy silt |
| P      | Peat                             |
| E      | Fine sand, silty sand lenses     |
| E'     | Sandy silt, clayey silt lenses   |
| F      | Sandy and clayey silt            |
| G      | Fine, locally silty sand         |

Figure A-1. Lido inlet – Typical soil profile.

As to the initial value of  $p'_{cio}$  it depends on the intrinsic compressibility characteristics ( $\lambda_i$  and  $v_{\lambda i}$ ) and the initial material state ( $e_0, p'_o$ ).

The relative initial position of the two surfaces is quantified by the model parameter  $X_{bo} = p'_{cno} / p'_{cio} - 1$ , which reflects the degree of the material interparticle bonding.

The plastic strains are calculated according to an associated flow rule and imposing the consistency condition which allows the current stress state to be always located on CS.

The viscous strains are calculated according to an associated flow rule in which the overstress of the current stress state with respect to the IS is taken into account.

The change in dimensions of the CS and IS is related to plastic and viscous strains according to appropriately defined hardening rules.

Moreover, the VISCO-CLAY model is characterized by the following parameters:

- $\lambda_n$  = slope of the Virgin Compression Line in the  $v$ - $\ln p'$  plane, being  $v = 1 + e$ , related to CS
- $\lambda_i$  = slope of the Virgin Compression Line in the  $v$ - $\ln p'$  plane, being  $v = 1 + e$ , related to IS
- $\kappa$  = slope of the Recompression Line in the  $v$ - $\ln p'$  plane B and G, respectively bulk and shear modulus, linked via Poisson ratio ( $\nu'$ ), allowing to compute elastic strains
- $\mu$  = parameter quantifying the component of the viscous strain rate when the current material state is located at or outside CS
- $\mu_{ur}$  = parameter quantifying the component of the viscous strain rate when the current material state falls between the IS and the CS
- $r_e$  = normalized radius of the elastic yield locus

Tab.A-1 reports the value of the model parameters used in the settlements calculations of fine grained soils, where:

- $\gamma$  = bulk density
- $\phi'$  = angle of shearing resistance
- $k_v$  = coefficient of hydraulic conductivity for flow in vertical direction
- $K_o$  = coefficient of the earth pressure at rest
- $\nu'$  = Poisson ratio

Table A-1. Parameters adopted for fine grained soils in settlements calculation.

| Stratum | $\gamma$<br>(kN/m <sup>3</sup> ) | $\sigma'_{vy}/\sigma'_{v0}$<br>(-) | $\phi'$<br>(°) | $K_0$<br>(-) | $v'$<br>(-) | $k_v$<br>(m/s) | $M$<br>(-) | $\kappa$<br>(-) | $\lambda_i$<br>(-) | $\lambda_n$<br>(-) | $\mu$<br>(-) | $v_\lambda$<br>(-) | $X_{bo}$<br>(-) | $\mu_{ur}$<br>(-) | $r_e$<br>(-) |
|---------|----------------------------------|------------------------------------|----------------|--------------|-------------|----------------|------------|-----------------|--------------------|--------------------|--------------|--------------------|-----------------|-------------------|--------------|
| B       | 19                               | 1.25                               | 32             | 0.526        | 0.2         | 1e-8           | 1.287      | 0.0047          | 0.110              | 0.085              | 0.0005       | 2.360              | 10              | 0.00040           | 0.20         |
| D       | 19.5                             | 1.15                               | 34             | 0.473        | 0.2         | 1e-9           | 1.375      | 0.0047          | 0.105              | 0.095              | 0.0002       | 2.335              | 10              | 0.00010           | 0.15         |
| E'      | 19                               | 1.10                               | 34             | 0.462        | 0.2         | 1e-9           | 1.375      | 0.0047          | 0.100              | 0.090              | 0.0010       | 2.300              | 12              | 0.00075           | 0.20         |
| F       | 19.5                             | 1.10                               | 34             | 0.462        | 0.2         | 1e-9           | 1.375      | 0.0040          | 0.100              | 0.092              | 0.0010       | 2.310              | 12              | 0.00075           | 0.25         |
| H       | 19                               | 1.10                               | 34             | 0.462        | 0.2         | 1e-9           | 1.375      | 0.0040          | 0.100              | 0.092              | 0.0010       | 2.310              | 12              | 0.00075           | 0.25         |

Table A-2. Parameters adopted for coarse grained soils in settlements calculation.

| Stratum            | $\gamma$<br>(kN/m <sup>3</sup> ) | $\phi'$<br>(°) | $K_0$<br>(-) | $M$<br>(-) | $G_0$<br>(MPa) | $G_0/G_{ur}$<br>(-) | $h_1$<br>(-) | $v'$<br>(-) |
|--------------------|----------------------------------|----------------|--------------|------------|----------------|---------------------|--------------|-------------|
| A                  | 19                               | 38             | 0.384        | 1.549      | 50             | 3.00                | 0.83         | 0.2         |
| C                  | 19                               | 38             | 0.384        | 1.549      | 70             | 1.90                | 0.83         | 0.2         |
| E (el. -40 to -50) | 18.5                             | 38             | 0.384        | 1.549      | 90             | 1.40                | 0.83         | 0.2         |
| E (el. -50 to -60) | 18.5                             | 38             | 0.384        | 1.549      | 120            | 1.30                | 0.83         | 0.2         |
| E (el. below -60)  | 18.5                             | 38             | 0.384        | 1.549      | 140            | 1.25                | 0.83         | 0.2         |
| G                  | 18.5                             | 36             | 0.412        | 1.462      | 180            | 1.40                | 0.78         | 0.2         |

$G_0$  = shear modulus from cross-hole tests

$G_{ur}$  = unload-reload modulus corresponding to the geostatic stress state

As to coarse grained material, predominantly fine sands and silty sands (strata E and G, see Fig.A-1), the elasto-plastic strain hardening model developed with the framework described in Li and Dafalias (2000) has been employed. The corresponding model parameters are reported in Tab.A-2, where:

$G_{ur}$  = unload reload shear modulus function of the material current state (i.e. of  $e$  and  $p'$ )

$K_p$  = plastic modulus, function of  $G_{ur}$ ,  $M$ ,  $h_1$  and  $\eta$ , being,  $h_1$  = hardening rule parameter and  $\eta = q/p'$ .

The values of  $\phi'$  corresponds to the peak angle of shearing resistance assuming linear Mohr-Coulomb strength envelope.

## ACKNOWLEDGMENTS

The authors express their thanks the Venice Water Authority (Agency of the Ministry for Infrastructures and Transportation) and to the Consorzio Venezia Nuova for consenting the presentation of this paper at the XVII ICSMGE in Alexandria.

The authors also acknowledge the great benefits and the deep insight achieved into the MOSE Project while serving as geotechnical consultants to the Consorzio Venezia Nuova and to the General Designer Technital Engineering during the site characterization and the design stage.

Special thanks and gratitude deserve Dr. L. Belloni of Technital and Prof. V. Fioravante from the University of Ferrara for their fruitful discussion and advices as well as for making available a mass of information and experimental data exposed in the paper.

Last but not least, the authors are thankful to the Geotechnical Groups of the University of Aquila, the University of Bologna and of GeorgiaTech, Atlanta for their meaningful contribution to the TTS characterization by means of advanced in situ tests.

## REFERENCES

Belloni, L. and Caielli, A. (1997). Origine dei Sedimenti a Malamocco. Atti Istituto Veneto di Scienze Lettere ed Arti, Tomo CLV (1996-1997), Venezia.

- Burghignoli, A., Jamiolkowski, M., Viggiani, C. (2007) Geotechnics for the preservation of historic cities and monuments: Component of a multidisciplinary approach. Special Lecture XIV European Conference on SMGE, Madrid, Vol 1 pp 3-38. Rotterdam: Millpress
- Burland, J.B. (1990). Piles as Settlement Reducers. XIX Convegno Nazionale di Geotecnica, A.G.I., Pavia, Vol.2, pp.21-24.
- Bonizzoni, F. and Da Prat, M. (2006). Internal Geotechnical Report, Studio Geotecnico Italiano, Milano
- Been, K., Jefferies, M.G. & Hachey, J. (1991). The critical state of sands. *Géotechnique*, 41 (3): 365-381.
- Been, K. & Jefferies, M.G. (1985). A state parameter for sands. *Géotechnique*, 35 (2): 91-112.
- Bolton, M.D. 1986. The strength and dilatancy of sands. *Géotechnique*, 36 (1): 65-78.
- Cola, S. & Simonini, P. (1999). Some remarks on the behaviour of Venetian silts, 2<sup>nd</sup> Int. Symp. on Pre-failure behaviour of geomaterials, IS Torino 99, pp. 167-174, Rotterdam: Balkema.
- Cola, S. & Simonini, P. (2002). Mechanical behaviour of silty soils of the Venice lagoon as a function of their grading properties. *Canadian Geotechnical J.*, 39 (4): 879-893.
- Fioravante, V., Giretti D. and Jamiolkowski M. (2007) Physical Modelling of Raft on Settlement Reducing Piles. Honoring Dr. John H. Schmertmann, ASCE GSP 180 pp. 206-229.
- Florin, W.A. (1956). Principles of Soil Mechanics. Moscow (in Russian).
- Gottardi, G. & Tonni, L. (2004). A comparative study of piezocone tests on the silty soils of the Venice lagoon (Treporti Test Site). ISC-2, Geotechnical and Geophysical Site Characterization, Porto, Vol. 2, pp. 1643-1649, Rotterdam: Millpress.
- Ishihara, K., Huang, Y. and Tshuchiya, H. (1998). Liquefaction Resistance of Nearly Saturated Sand Correlated with Longitudinal Wave Velocity. *Poromechanics*, pp.583-586. Rotterdam: Balkema.
- Jamiolkowski, M. (1999). Where are we going? Pre-failure Deformation Characteristics of Geomaterials, IS Torino, Vol.2, pp.1251-1262, Rotterdam: Balkema.
- Kovari, K. & Amstad, C. (1982). A new method of measuring deformations in diaphragm walls and piles. *Geotéchnique*, 22(4): 402-406.
- Li X.S. & Dafalias Y.F. (2000), Dilatancy for cohesionless soils, *Géotechnique* 50, n°4, pp.449-460.
- Leroueil, S. & Hight, D.W. (2002). Behaviour and properties of natural soils and soft rocks. Overview paper. Characterization and Engineering Properties of Natural Soils, Vol. 1, pp. 29-254, Tan et al. eds., Swets and Zeitlinger, The Netherlands.
- Mandolini, A., Russo, G. and Viggiani, C. (2005). Pile Foundations: Experimental Investigation, Analysis and Design. XVI ICSMGE, Osaka, Japan, Vol.1, pp.177-213, Rotterdam: Millpress.
- Marchetti, S., Monaco, P., Calabrese, M. & Totani, G. (2004). DMT-predicted vs. measured settlements under a full-scale instrumented embankment at Treporti (Venice), Italy. ISC'02, Geotechnical and Geophysical Site Characterization, Porto, Vol. 2, pp. 1511-1518, Rotterdam: Millpress.
- Mayne, P. & McGillivray, A. (2004). Seismic piezocone and seismic flat dilatometer tests at Treporti. ISC'02, Geotechnical and Geophysical Site Characterization, Porto, Vol. 2, pp. 1695-1701, Rotterdam: Millpress.
- Mesri, G. & Godlewski, P. M. (1977). Time- and stress- compressibility relationship. *JGED*, ASCE, 105(GT5): 417-430.
- Mesri, G., Shahien, M. & Feng, T.W. (1995). Compressibility parameters during primary consolidation. Int. Symp. On Compression and Consolidation of Clayey Soils – IS Hiroshima '95, Hiroshima, vol. 2, pp. 1021-1037. Rotterdam: Balkema

- Randolph, M.F. and Wroth, C.P. (1978) An analysis of the vertical deformation of pile groups. Technical Report CUED/D-SOILS/TR 59, Cambridge University, Engineering Department, Geotechnical Group.
- Ricceri, G. (2007). Il ruolo della geotecnica nella salvaguardia di Venezia e della sua Laguna. Croce Lecture, 7a edizione. Rivista Italiana di Geotecnica, 41(1), 12-52
- Ricceri, G., Simonini, P. & Cola, S. (2002). Applicability of piezocone and dilatometer to characterize the soils of the Venice lagoon. Geotechnical and Geological Engineering, 20 (2): 89-121.
- Rocchi, G., Fontana, M. and Da Prat, M. (2003). Modelling of Natural Soft Clay Destruction Process Using Viscoplasticity Theory. Géotechnique, 53 (8), 729-745.
- Rocchi, G., Fontana, M. and Da Prat, M. (2005). Personal communication.
- Russo, G. (1998). Numerical Analysis of Piled Rafts. Int. Journal of Numerical and Analytical Methods in Geomechanics, 22 (6) 477-493.
- Simonini, P. (2004). Characterization of the Venice lagoon silts from in-situ tests and the performance of a test embankment. Keynote Lecture. ISC'02, Geotechnical and Geophysical Site Characterization. Porto, 1, pp. 187-207, Rotterdam: Millpress.
- Simonini, P., Ricceri, G. & Cola, S. (2006). Geotechnical characterization and properties of the Venice lagoon heterogeneous silts. Invited Lecture. 2<sup>nd</sup> Int Workshop on Characterization and Engineering Properties of Natural Soils. Singapore, vol. 4, pp. 2289-2328. London: Taylor & Francis
- Tochnog (1989). A free explicit/implicit GFE program, developed by FEAT, Finite Element Application Technology (<http://tochnog.sourceforge.net>).
- Valle-Molina, C. (2006). Measurements of  $V_p$  and  $V_s$  in Dry, Unsaturated and Saturated Specimens with Piezoelectric Transducers, Ph. D. Dissertation, the University of Texas at Austin.
- Viggiani, C. (1998). Pile Groups and Piled Rafts behaviour. BAP III Int. Geot. Sem. Deep Foundations on Bored and Auger Piles, Ghent, pp. 77-94, Rotterdam: Balkema
- Viggiani, C. (2001). Analisi e progetto delle fondazioni su pali. I Arrigo Croce Lecture, Rivista Italiana di Geotecnica 35, (1), 17-46.
- Wood, D., Belkeir, K. & Liu, D.F. (1994). Strain softening and state parameter for sand modelling. Géotechnique, 44 (2): 335-339.
- Wroth, C.P. & Bassett, R.H. (1965). A stress-strain relationship for the shearing behaviour of sand, Géotechnique, 15 (1): 32-56.
- Zeevaert, L. (1972). Foundation Engineering for Difficult Subsoil Conditions. New York: Van Nostrand Reinhold Company